University of Tennessee, Knoxville
Trace: Tennessee Research and Creative Exchange

Masters Theses | Graduate School

8-2018

Candidate Measurement Technique Application as a Method for Materials Accountancy in Electrochemical Reprocessing

Stephen N. Gilliam
University of Tennessee, zln179@vols.utk.edu

Recommended Citation

Gilliam, Stephen N., "Candidate Measurement Technique Application as a Method for Materials Accountancy in Electrochemical Reprocessing. " Master's Thesis, University of Tennessee, 2018.
https://trace.tennessee.edu/utk_gradthes/5171

This Thesis is brought to you for free and open access by the Graduate School at Trace: Tennessee Research and Creative Exchange. It has been accepted for inclusion in Masters Theses by an authorized administrator of Trace: Tennessee Research and Creative Exchange. For more information, please contact trace@utk.edu.

To the Graduate Council:

I am submitting herewith a thesis written by Stephen N. Gilliam entitled "Candidate Measurement Technique Application as a Method for Materials Accountancy in Electrochemical Reprocessing." I have examined the final electronic copy of this thesis for form and content and recommend that it be accepted in partial fulfillment of the requirements for the degree of Master of Science, with a major in Nuclear Engineering.

Jamie B. Coble, Major Professor

We have read this thesis and recommend its acceptance:

Lawrence H. Heilbronn, Steven E. Skutnik

Accepted for the Council:
Dixie L. Thompson

Vice Provost and Dean of the Graduate School

(Original signatures are on file with official student records.)

Candidate Measurement Technique Application as a Method for Materials Accountancy in Electrochemical Reprocessing

A Thesis Presented for the
Master of Science
Degree
The University of Tennessee, Knoxville

Stephen N. Gilliam
August 2018

Copyright © 2018 by Stephen Nathaniel Gilliam
All rights reserved.

ACKNOWLEDGEMENTS

This research was supported by a Nuclear Energy University Programs (NEUP) grant sponsored by the U.S. Department of Energy. This thesis also encompasses collaboration between the University of Tennessee, Knoxville and Sandia National Laboratory (SNL).

Furthermore, I would like to extend special gratitude and acknowledge my research advisor, Dr. Jamie Baalis Coble and also the other members of the defense committee, namely, Dr. Steven Eugene Skutnik and Dr. Lawrence Harvey Heilbronn.

ABSTRACT

Electrochemical reprocessing is a promising method to recover useful fissile material from spent nuclear fuel. Due to the recent attention surrounding electrochemical reprocessing as a complement or alternative to aqueous methods, necessary safeguards must be developed. However, the process requires high temperatures and an inert atmosphere thus complicating the prospect of making material accountancy measurements. Thus, to be deployed commercially, viable material accountancy and process monitoring methods must be designed and tested to meet safeguard standards. This work focuses on gamma spectroscopy and total neutron counting methods, which have previously been applied to aqueous reprocessing. These signatures are simulated in a previously developed flowsheet model. By tracking the isotopic mass concentrations at a given time and location, proper emission rates can be calculated that yield accurate representations of the material. Furthermore, notional diversion scenarios were simulated to evaluate the sensitivity of the measurement simulations to slight changes in material mass. Confirmatory measurements at key locations allowed for identification and differentiation of normal and off-normal operating conditions.

TABLE OF CONTENTS

LIST OF TABLES

LIST OF FIGURES

CHAPTER 1: INTRODUCTION

Electrochemical reprocessing was developed as a method to enhance efficiency and reduce waste production when separating major actinides from used nuclear fuel (UNF). The development of a separate process from aqueous methods was deemed necessary in order to handle newer and hotter fuel types. In contrast to aqueous processes, wherein the separation action is driven by manipulation of the redox state of actinides in order to transfer selected species from an aqueous phase to an immiscible organic phase, extraction in electrochemical separation is driven by differences in the Gibbs Free Energy of the actinide constituents dissolved into the molten salt electrolyte. It uses high temperature electrorefining as the separation mechanism originating from the development of the Integral Fast Reactor (IFR) program at Argonne National Laboratory (ANL) [1]. This process coextracts plutonium in with other minor actinides and transuranics (TRU), which increases the difficulty of using it as weapons grade material, increasing proliferation resistance. Electrochemical reprocessing can save disposal space, reduce the radiotoxicity of spent fuels, and increase uranium utilization efficiency [2].

While electrochemical reprocessing shows promise as a method of recovering valuable fissile material from fresher discharged fuel from a reactor, safeguards measurement methods must be developed to ensure material accountancy. Four key differences between aqueous and electrochemical reprocessing that present challenges to safeguards are: the lack of an accountability tank, the inability to flush out the plant, quantifying the electrorefiner inventory, and accurately measuring the backend product [3]. Research is being done across the globe in countries such as the United States, France, Russia, South Korea, and Japan to develop these specific safeguards that will make electrochemical reprocessing a more viable and proliferation resistant method [1], [4], [5] . These safeguards, while

protecting against loss of nuclear material, also have the added benefit of providing a method to check on the performance of the facility.

To further the development of safeguards, the separations and safeguards performance electrochemical (SSPM EChem) model has been developed at Sandia National Laboratory (SNL) [3]. This system models the major components of the electrochemical processes and was used to model current safegurdas methods applied in commercial aqueous operations. The purpose of this research is to evaluate gamma and neutron spectroscopy for safeguards in electrochemical reprocessing facilities. This will be done by using the Origen database developed by Oak Ridge National Laboratory to parse out nuclear data pertinent to such calculations [6].

1.1 Organization of the Document

The next chapter reviews the relevant literature in electrochemical reprocessing development as well as the fundamental physics of gamma and neutron spectroscopy. Subsequent chapters then outline the specific problem addressed by this work and the methodology proposed to solve this problem. Finally, the results of application of this methodology to three available locations within a previously-developed flowsheet model. Concluding remarks, as well as proposed areas of future work which do not fall under the scope of this thesis, are also given.

CHAPTER 2: BACKGROUND

Electrochemical reprocessing, also known as pyroprocessing, is a proposed alternative to the commercially used aqueous, mainly PUREX (Plutonium and Uranium Extraction), reprocessing method. It is a process that relies on the differences in Gibbs free energy of the metallic fuel and fission products to separate the UNF into reusable products. The process is outlined in a flowchart in Figure 1 for the multiple components of the cycle [2]. The process can be broken down into five key components: preprocessing, electroreduction, electrorefining, cathode processing, and salt purification. This review is meant to examine this process as a whole and describe probable candidate measurement techniques that can aid in material accountancy and safeguards.

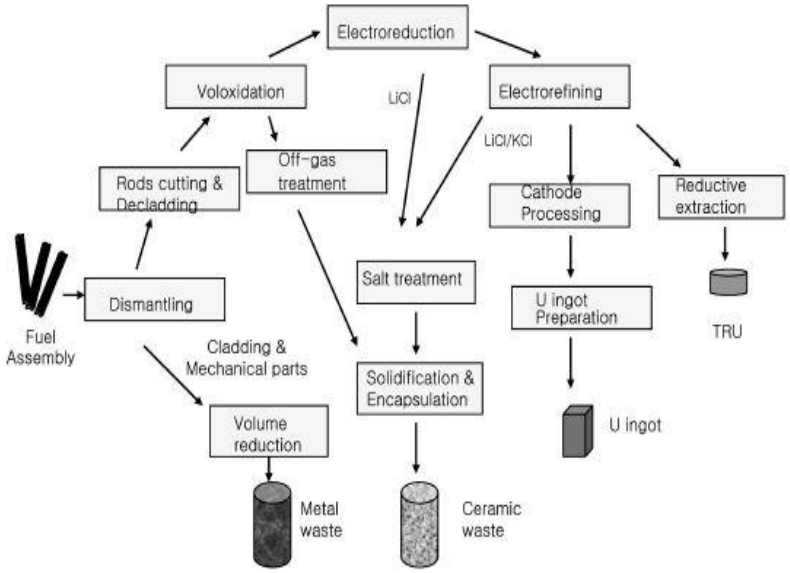

Figure 1: Processing steps of pyroprocessing spent fuel [2].

2.1 Electrochemical Reprocessing

2.1.1 Preprocessing

The beginning phase sees the fuel assemblies disassembled by the removal of fuel rods that are then cut to a short length. The shortened segments are then cut again in the axial direction until an appropriate size is reached. Fuel pellets of uranium oxide (UO_2) are then collected from the cladding and transported to the subsequent voloxidation (volumetric oxidation) process [7], wherein voloxidation UO_2 is oxidized to produce U_3O_8 powder. The fuel cladding is transported to the metal waste treatment cell. Voloxidation results in a powdered fuel form which increases the surface area and thus providing a higher rate of electroreduction. This is done by decreasing the density, thereby increasing the volume. Most of the gaseous fission products, such as tritium, krypton, and xenon are sent to an off-gas treatment system [7]. To prevent small powders from being siphoned to the off-gas collection system, the flow rate of air is maintained below a certain threshold. This completes the transformation of the fuel into a suitable form to be used as feed material into the electrolytic reduction process.

2.1.2 Electrolytic Reduction

Before the fuel can enter the electrorefiner it must be reduced to transform it into a metallic form if it was originally an oxide fuel. In this step, oxides of actinides and noble metals are reduced to metallic form. Figure 2 demonstrates this process where a molten salt LiCl-Li_2O is used as the electrolyte. The cathode containment wall is usually composed of a magnesia membrane which allows the ions to flow

in and out during the redox reaction. It is shown that Li_2O dissociates where the oxygen ions are then collected at the anode. The newly-formed lithium then accumulates at the cathode and reduces the metal oxides to metal chlorides [7].

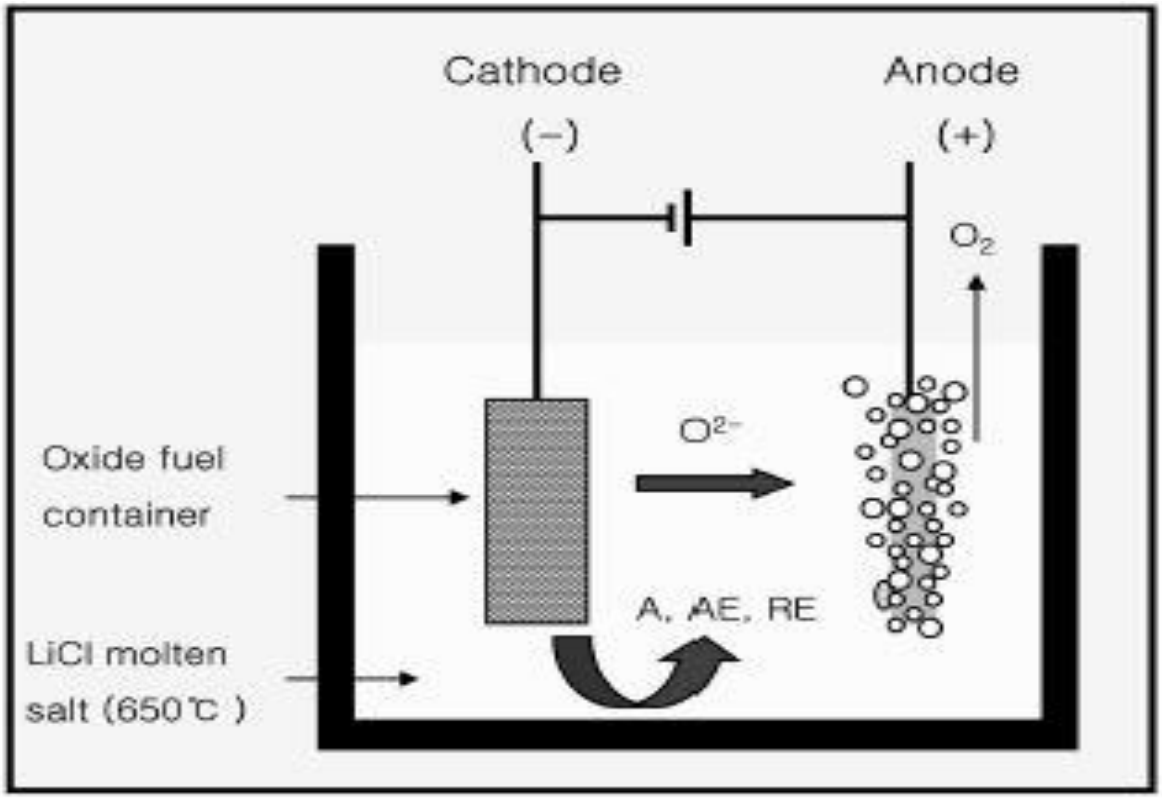

Figure 2: Example demonstrating the electroreduction process [2].

2.1.3 Electrorefining

After reduction, the metal chlorides are used as feed into the electrorefiner where recovery of uranium and TRU occurs. The fuel is placed in an anode basket and dispensed in a pool of LiCl-KCl salt maintained at 450-500 °C [1]. Uranium and TRU are then chlorinated at the anode and deposited into the salt. From there deposition onto a cathode is controlled by adjusting the cell voltage, demonstrated

in Figure 3. The alkaline and alkaline earth constituents form stable chlorides and thus stay within the salt throughout the refining process. The noble metal chlorides tend to stay in metallic form and reside at the anode due to having a lower free energy for formation [7]. After recovery of uranium at the solid cathode, in which the uranium is reduced back to metallic form, the cell voltage is adjusted to collect uranium and TRU onto a separate liquid cadmium cathode (LCC). This is done to preserve the uranium content on the solid cathode and prevent contamination from TRU. Remaining fission products segregate between the anode basket and the molten salt while noble metals, such as rhodium and ruthenium, remain in the anode basket [1].

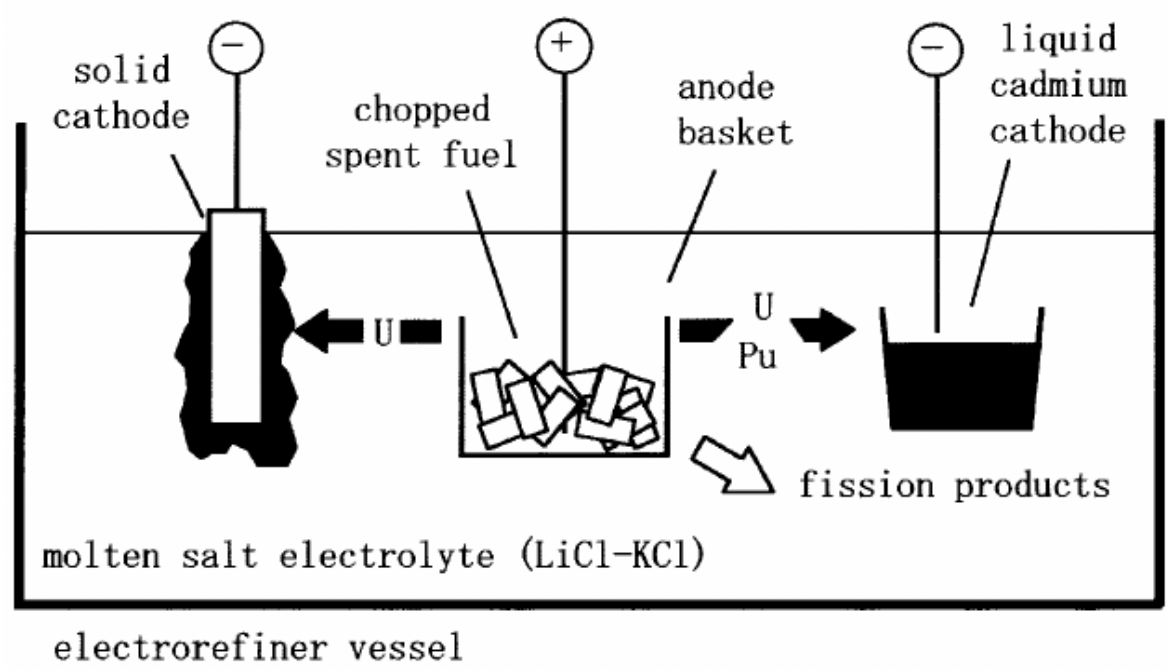

Figure 3: Demonstration of the migration for uranium and TRU products during the electrorefining process [3].

2.1.4 Cathode Processing

The molten salt that accompanied the uranium and TRU is removed by vacuum distillation and goes to the salt purification cycle. The uranium and TRU are then cast in ingot form through a cathode processing system with parameters of 1200 °C and pressures of 1 torr. This process also takes the remaining material from the anode basket, such as undissolved actinides, salt, and noble metals, and loads them into a heated vacuum distillation furnace that is used to consolidate the metals into an ingot form [1].

2.1.5 Salt Purification

Since the salt from electroreduction and electrorefining processes is proposed to be in a state of continuous flow, part of it must be circulated through a purification process before being recycled to each respective process again [7]. There is also salt waste that comes in two forms, LiCl from the reduction process and LiCl-KCl from refining [8]. These used salts are highly radioactive and heat-generative and must be properly disposed of. Currently the salt is stored in a glass-bonded sodalite ceramic waste form. This is done by milling the salt into a fine particulate and then absorbing it into zeolite-4A. Then a borosilicate glass binder mixes the salt-loaded zeolite and heats it to 915-950 °C [1]. This salt waste production method is seen as a wasteful approach and research is being done to minimize salt waste [8].

2.2 SSPM EChem Model

The SSPM EChem model is a continuous event model developed in the MATLAB/Simulink software at SNL. This software package uses blocks to represent the conditions for which the processes involved in pyroprocessing go through during facility operation. The system tracks the mass flow rate in kg/sec of elements with atomic numbers ranging from 1 to 99. The total mass flow rate of the molten salt is tracked separately from its elemental constituents [3]. The model is broken down into four distinct areas: three material balance accountancy (MBA) areas shown in Figure 4 and a process monitoring section. The MBA areas start off with the front-end process which include the UNF storage and the shredding and voloxidation processes. This models the preprocessing steps required to convert the fuel to U_3O_8 such that it can be put through the

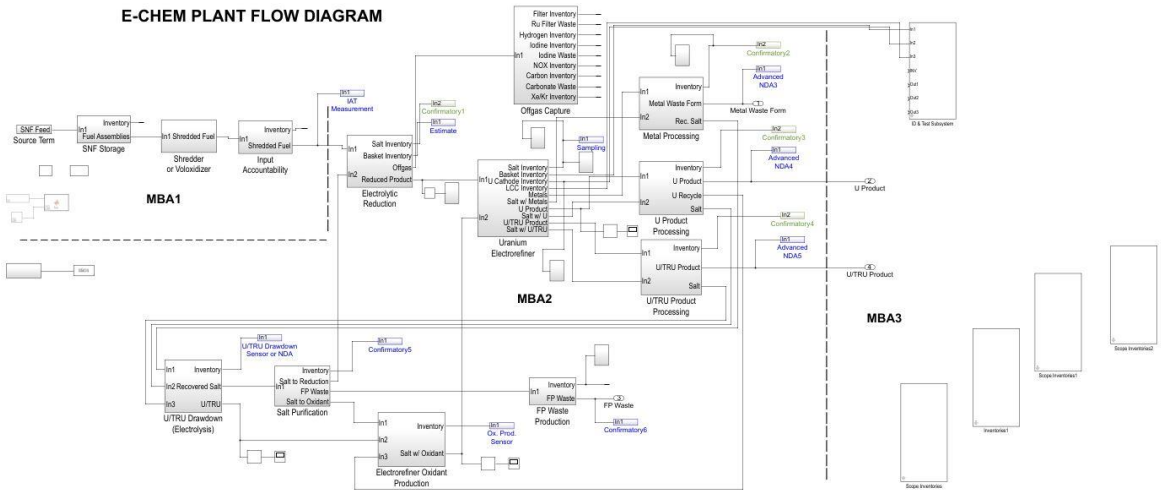

Figure 4: Flow diagram outlining the MBA areas throughout the SSPM EChem model [3].

electrolytic reducer. The second MBA begins with the reduction process and simulates the transformation of the fuel into a metallic form. Next, the electrorefining process described earlier is modeled. The model assumes that the cathode containing uranium is 100% uranium. The LCC containing uranium and TRU is assumed to be 70% uranium and 30% TRU [3]. The metal processing unit also assumes no actinide flow into it. The last process in the second MBA is the recycling of the molten salt back to the electrolytic reducer and electrorefiner. This also includes an actinide drawdown stage for subsequent fission products to be put in an appropriate waste form [9]. The final MBA area is used to keep inventory of everything tracked throughout the pyroprocessing process by collecting and storing all the variable outputs from the model.

2.2.1 SSPM EChem GUIs

Currently, the model allows multiple user inputs to account for various fuel types, discharge times, simulation time, and diversion scenarios. A visual of the user interface is given Figure 5. The upper portion accounts for fuel parameter selection where one of nine different enrichment and burnup combinations can be selected, including, and five different discharge times for each combination. Next is the duration, in hours, for the simulation of the facility to be run. The bottom portion of Figure 5 controls the different diversion scenarios considered by the model. The location for diversion to occur is selected from 11 locations, including the SNF storage, shredder, and all nine locations within MBA2. Next, the start and end times for the diversion are specified within the total simulation time. Finally, the percent of material that will be diverted is selected along with the type of diversion as being either direct or U substitution.

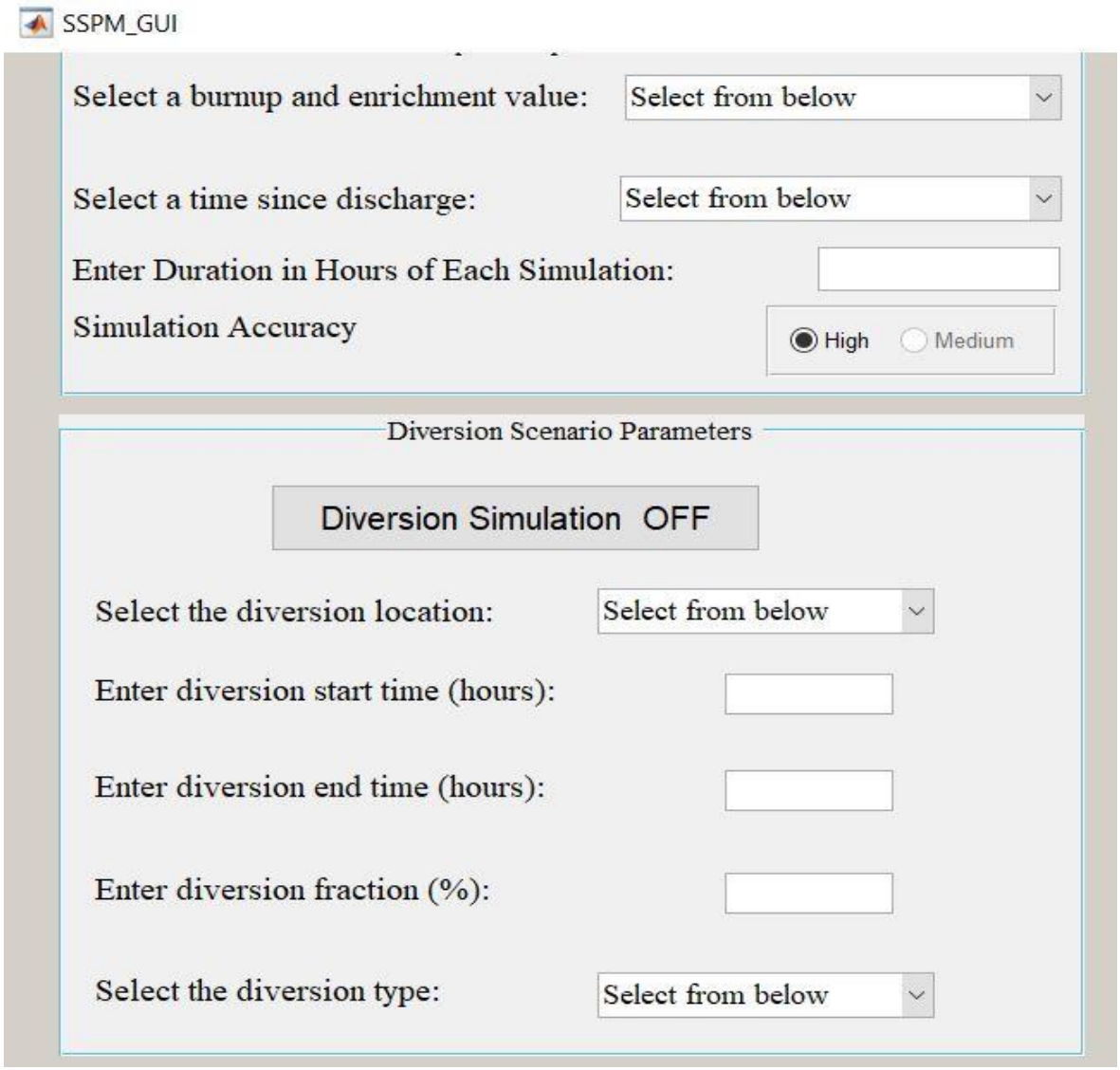

Figure 5: SSPM simulation scenario GUI.

The second GUI, shown in Figure 6, aids in the organization of an easily readable excel file that summarizes elemental and isotopic information. It allows the user to select multiple data sets, including inventory and process monitoring tests, and the location from which the data is pulled from to be put into the excel file. The last information is the selection of the specific elements and their isotopes that the user requests the information for. This section is organized in the shape of a periodic table with the elements symbols being tracked highlighted in blue and the ones not being tracked in black.

2.2.2 Process Monitoring and Safeguards

Due to the differences in operation that arise with pyroprocessing, compared to aqueous methods, accountancy and process monitoring requirements must be updated from existing regulations to have adequate performance. This holds true for every step of the process but major safeguard elements that must occur are outlined below stemming from the most recently constructed plant, Rokkasho in Japan [3]:

- Defined MBAs for nuclear material accounting.
- Key Measurement Points (KMPs) for measuring flow and inventory of material.
- Defined strategic points for containment, surveillance, and verification measures.
- Nuclear material accountancy supported by review of operating records and state reports.
- Annual Physical Inventory Verification at a shutdown and flushout.

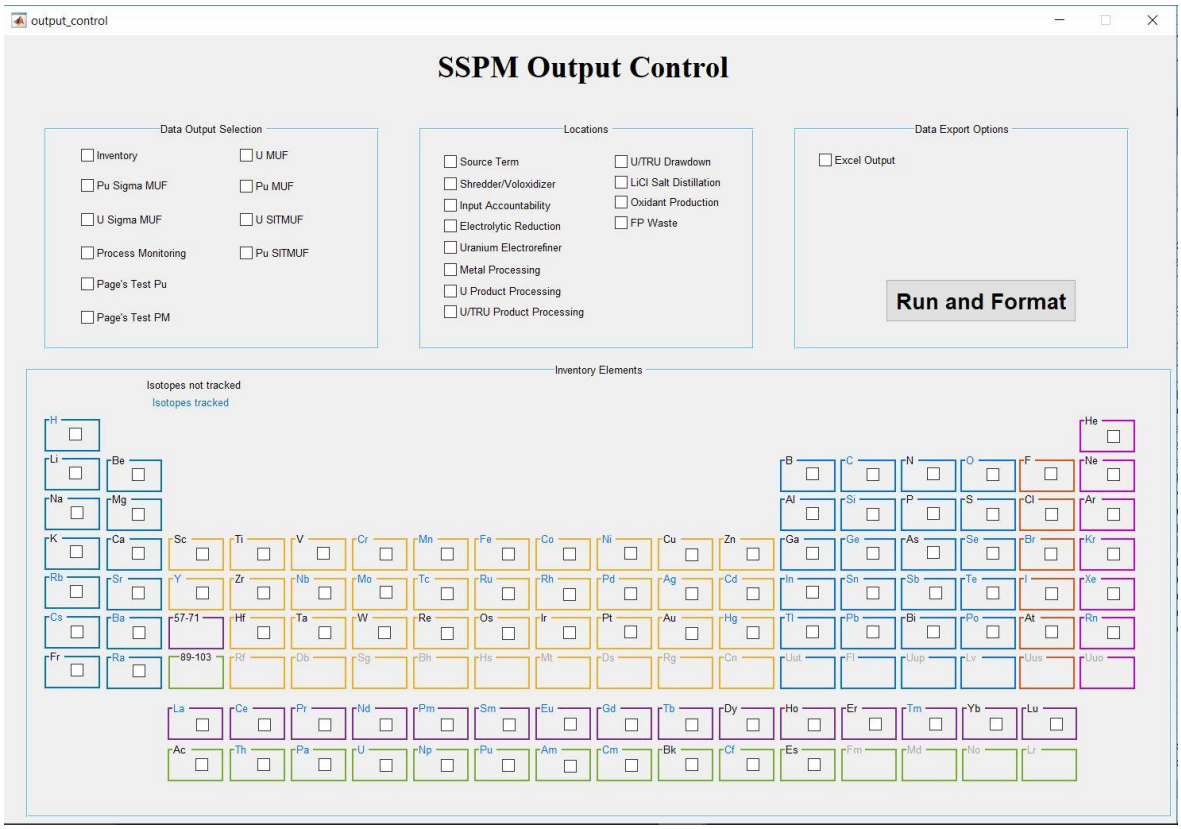

Figure 6: SSPM output control interactive interface.

- Routine monthly Interim Inventory Verification for timely detection of diversions.
- Verification of domestic and international transfers of nuclear material.
- Statistical evaluation of the material balance to determine Material Unaccounted for (MUF).
- Verification of facility design information.
- Verification of the operator's measurement system.
- +Additional continuity of knowledge over the plutonium-bearing material
- Routine monthly Interim Inventory Verification for timely detection of diversions.
- Verification of domestic and international transfers of nuclear material.
- Statistical evaluation of the material balance to determine Material Unaccounted for (MUF).
- Verification of facility design information.
- Verification of the operator's measurement system.
- Additional continuity of knowledge over the plutonium-bearing material using the Solution Monitoring System and the Plutonium Inventory Measurement System.
- Short interval verification, analyzing samples every ten days to provide additional assurance against diversion.
- Frequent evaluation of the nuclear material balance using Near Real Time Accountancy (NRTA).

The SSPM EChem model's process monitoring section, shown in Figure 7, uses detailed simulated measurements to calculate inventory differences (IDs), mainly with regards to plutonium content for each processing unit. The process monitoring subsection uses an embedded MATLAB script for calculating the IDs, the cumulative sum (CuSum) ID, standard error of inventory difference (SEID), and the Page's Test [3].

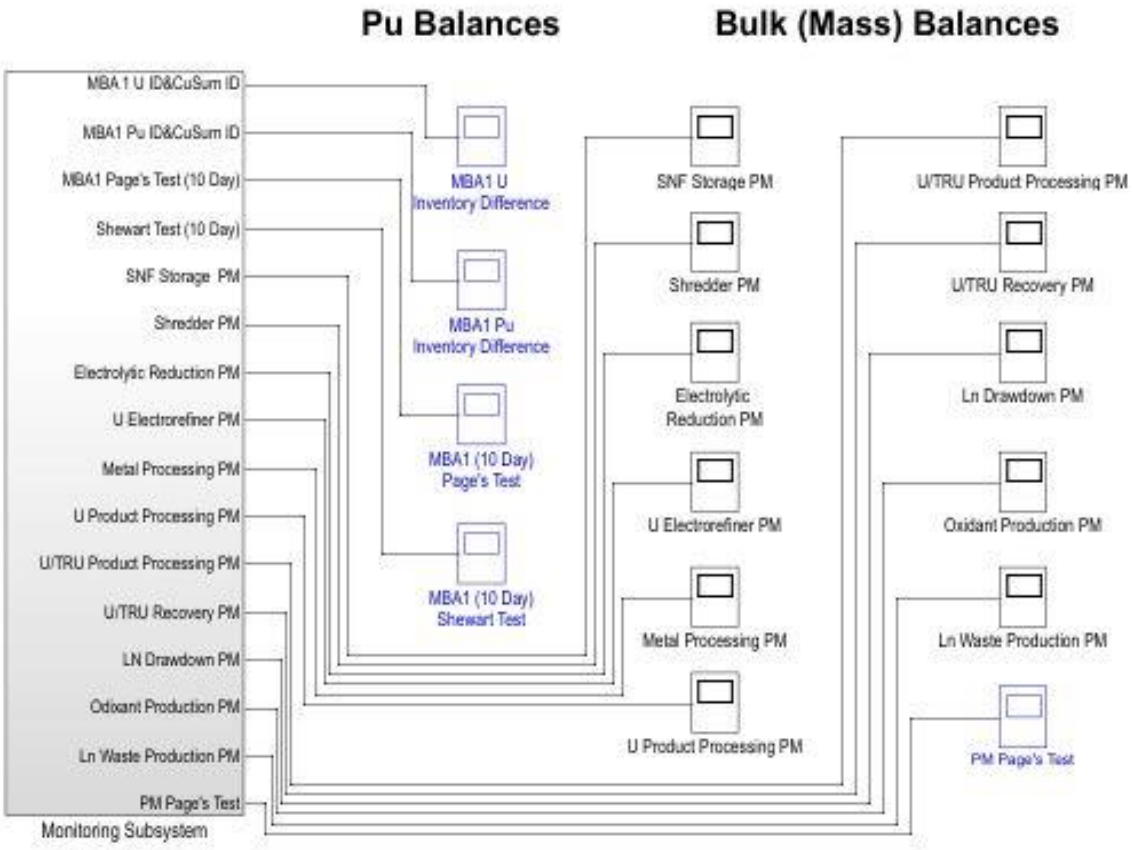

Figure 7: Process monitoring subsection of the SSPM EChem model [3].

The model was tested and has been reviewed by researchers at Argonne National Laboratory to ensure that flows and inventories are adequate representations [3]. The measurements act as expected in diversion and non-diversion cases. At this stage in the research, it provides enough information to show what measurement uncertainties will meet regulatory requirements.

2.3 Candidate Measurements

2.3.1 Overview

Using the SSPM EChem model, two radiation based signatures will be discussed, gamma and neutron emission. To aid in the simulation of these signatures, it is useful to examine previous research and application specifically for pyroprocessing. What follows is a brief discussion of the fundamental principles of each technique and how it can apply to pyroprocessing. Material that will be highlighted are the physics and detection systems for each technique. This section is designed to give background regarding each technique's fundamental principles and discuss their implementation within the SSPM EChem model or similar pyroprocessing facility models.

2.3.2 Gamma Spectroscopy

Gamma detection plays a significant role in material accountancy as many fission products and actinides emit gamma rays or photons upon decay. It is a non-destructive technique that can strengthen the capability to verify the gross and

isotopic inventory of UNF throughout the reprocessing cycle. The capability of isotopic identification stems from the characteristic energies that gamma rays display when emitted from individual radionuclides [10]. The production of gamma rays comes when a nucleus moves from an excited state to the ground state. This can be done in one transition or many and the energy and number of gamma rays produced depends on the differences in nuclear energy levels resulting in a unique signature for each isotope. Although it will not be discussed further in this work, it is important to note that a complimentary particle is that of an x-ray which spans roughly the same frequencies on the electromagnetic spectrum as gamma rays and only differs in its origin [10]. X-rays are not formed by transitions of the nucleus but by the transitions electrons make to different orbitals. Once a gamma or x-ray has been emitted there are three ways it can interact with an atom; the photo-electric effect, Compton scattering, and pair production. Each of these three interaction methods produce either subsequent gamma rays or secondary particles. It is important to understand these mechanics as they aid in identifying spectral gamma ray features, thus helping identify various radioisotopes.

In the photoelectric effect all the energy of an incident gamma ray is transferred to an electron located near the nucleus of an atom, predominately in the K and L-shells [10]. The energy transferred must be enough to overcome the electron's binding energy, while the rest of the gamma ray energy goes to the atom to conserve momentum. The electron is then ejected from the atom, resembling a β-particle, which can then cause secondary ionization within the medium. This mechanism is predominately used in radiation detection to identify isotopes that emit gamma rays of a signature energy.

In Compton scattering, the gamma ray transfers part of its energy to an outer shell electron as opposed to all of its energy to an inner shell. The electron is then ejected from the atom and it and the gamma ray are scattered with direction and energy dependent on the initial energy of the gamma ray. Since the electron occupies an outer shell, its binding energy is considered relatively weak. This allows for the assumption that the energy gained by the electron is equal to that lost by the gamma ray. The scattering angle can range from 0° to 180° and thus detection systems capture a wide energy range of pulses, known as the Compton continuum [11].

The final gamma interaction is pair production in which two gamma rays, each of energy 511 keV, are emitted in the process. This occurs when an initial gamma incident on an atom has energy over 1022 keV. Once the gamma ray is near the electromagnetic field of a nucleus, the energy can be converted into an electron-positron pair. When the positron travels through the medium and annihilates with an electron the result is two gamma rays of equal energy emitted in opposite direction.

Once an interaction process has occurred, it must be recorded to verify the content of the medium. This can be done by using a multitude of detectors. The ones commonly used in non-destructive analysis are those whose signal outputs are proportional to the energy deposited by the gamma ray, such as gas-filled, scintillators, solid-state detectors, and HPGe detectors [11]. The efficiency of such techniques is usually within ten percent, whether it is via passive gamma or total counting methods [12]. The main locations within the system where gamma detectors would be deployed are the electrorefiner, processing units, and at the headend for input accountancy.

2.3.3 Total Neutron Counting

Total neutron counting, analogous to gross gamma counting, involves the quantification of three categories of neutrons: prompt neutrons produced from spontaneous fission events, delayed neutrons, and (α,n) reactions which occur primarily in low-Z material. The production of both spontaneous and delayed neutrons come from fission sources. This occurs when a heavy element either decays or is bombarded with thermal neutrons. The result yields lighter elements, called fission products, and an average of 2-3 prompt neutrons with energies around 2.3 MeV [13]. An example of this process is shown in (1) where Pu-239 is fissions to produce Pd-112 and Cd-124. The initial neutrons produced are labeled prompt because they are produced instantaneously, within 10^{-14} seconds, as the fission event occurs. Delayed neutrons are also a byproduct of fission events and arise after one of the fission products undergoes radioactive decay, usually beta decay. The resulting nuclide is left in an excited state and when the state is high enough a neutron, known as a delayed neutron, is ejected. The label of “delayed” stems from the time it takes for the fission product to beta decay.

$$^{239}_{94}Pu \rightarrow \ ^{112}_{46}Pd + \ ^{124}_{48}Cd + \ 3^{1}_{0}n \qquad (1)$$

The last major neutron source, (α,n) reactions, happen when alpha decays occur in the presence of light element material, producing fast neutrons in the MeV energy range [13]. An example reaction is seen in (2) where the element beryllium is hit by an alpha particle to produce a single neutron and gamma ray. Historically (α,n) reactions have played a lesser role in quantifying actinides as the emission have been overshadowed in magnitude when compared to spontaneous fission.

Due to the amount of salt present within the electrochemical cycle, and it containing target elements for the alpha particles to interact with, this method may prove to be a significant neutron tracking procedure.

$$^{9}_{4}Be + {}^{4}_{2}He \rightarrow {}^{12}_{6}C + {}^{1}_{0}n + \gamma \quad (2)$$

Total neutron counting is a non-destructive method that has been used for safeguards worldwide for decades [14]. This technique holds an advantage over that of total gamma counting when it comes to estimating burnup due to gamma rays being more attenuated than neutrons [15]. The precision of total neutron counting typically spans between one and two percent error [14]. For these reasons, this technique is useful and should be considered a candidate to be deployed within the electrorefiner, processing units, and for input accountancy to monitor the neutron yields predominately from curium, americium, and plutonium.

CHAPTER 3: SIMULATION DEVELOPMENT

Simulation was done for two separate signatures, gamma and total neutron emissions. The gamma simulation used only discrete gamma lines as they were deemed sufficient as a more realistic measurement model would significantly impact the EChem runtime. Next, total neutron emissions were broken down into two parts, spontaneous fission and (α,n) reactions. Delayed neutrons were left out due to the minuscule impact they would have in regard to the emission rate spectrum.

3.1 Gamma Emissions

The Origen.rev04.mpdkxgam file from SCALE-6.2 was used to parse the energy and intensity for gamma rays for the isotopes being tracked in the SSPM EChem model. This file gives x-ray, discrete gamma ray, and pseudo gamma information but only the discrete gamma lines were needed to simulate the gamma emission rate. The file also contained the half-life for each isotope which was needed to calculate each isotope's activity. An example of the gamma emission data is shown in Figure 8. The header record for each nuclide contains the nuclide ID, the total number of emission lines in the evaluation, as well as the number of discrete x-ray lines, discrete gamma lines, and number of pseudo lines used to represent continuum data if present in an evaluation used to reconstruct continuous energy emission spectra from the discrete representation [6]. The last entries in the header include the total gamma energy in MeV and the nuclide name. The emission spectrum is listed using pairs of entries for the photon energy in MeV and associated photon emission in photons per disintegration.

```
571400          52.       14.       38.        0.        0.2.3083E+00     1a   140
           4.3847E-03 2.1017E-04 4.8247E-03 1.7789E-03 5.3304E-03 1.5654E-03
           6.0946E-03 2.3418E-04 3.4291E-02 5.9015E-03 3.4743E-02 1.0817E-02
           3.9196E-02 1.0523E-03 3.9285E-02 2.0389E-03 3.9550E-02 1.2513E-05
           3.9570E-02 1.6866E-05 4.0227E-02 2.2404E-04 4.0247E-02 4.3591E-04
           4.0340E-02 2.6312E-06 4.0344E-02 3.5410E-06 2.4595E-02 1.4971E-05
           6.4135E-02 1.4310E-04 6.8916E-02 7.5366E-04 1.0942E-01 2.1942E-03
           1.3112E-01 4.6746E-03 1.7354E-01 1.2688E-03 2.4193E-01 4.1404E-03
           2.6654E-01 4.6555E-03 3.0690E-01 2.4804E-04 3.2876E-01 2.0320E-01
           3.9752E-01 7.3458E-04 4.3249E-01 2.9002E-02 4.3850E-01 3.9114E-04
           4.4550E-01 2.8620E-05 4.8702E-01 4.5506E-01 6.1812E-01 3.7206E-04
           7.5164E-01 4.3312E-02 8.1577E-01 2.3278E-01 8.6785E-01 5.5046E-02
           9.1955E-01 2.6617E-02 9.2519E-01 6.8974E-02 9.5099E-01 5.1898E-03
           9.9290E-01 1.3356E-04 1.0451E+00 2.4804E-04 1.0972E+00 2.2896E-04
           1.3035E+00 4.1976E-04 1.4052E+00 5.9148E-04 1.5962E+00 9.5400E-01
           1.8773E+00 4.1022E-04 1.9246E+00 1.3356E-04 2.0832E+00 1.1543E-04
           2.3479E+00 8.4906E-03 2.4641E+00 1.1448E-04 2.5214E+00 3.4630E-02
           2.5473E+00 1.0112E-03 2.8996E+00 6.6780E-04 3.1185E+00 2.4804E-04
           3.3204E+00 3.8160E-05
```

Figure 8: Gamma resource format example showing La-140 decay photon emission [6].

Once the energies and intensities were parsed from the file, they were binned into 1024 channels with the 1024th channel including energies above the high cutoff. The complete energy distribution ranged from 0 to 5 MeV and was binned evenly across the 1023 open channels resulting in an energy width of 4.88 KeV. The decay constants (λ) for each isotope was obtained using the half-life from the previously mentioned file. The decay constant is used to calculate the activity of each isotope. This isotopic gamma and decay constant information was then loaded into the SSPM EChem model via a Simulink function block where the calculations below occur to receive the gamma signatures (absolute emission rate) on an isotopic level. Equation (3) demonstrates how to calculate the number of atoms for a given isotope. The mass being tracked is in kg and must first be converted to grams in order to divide by the respective atomic mass and multiplied by Avogadro's constant. These isotopic atom quantities are then multiplied by the decay constant in equation (4) to obtain the activity of each isotope at each given location throughout the model. This method will be used throughout the other modeling sections to obtain activity when needed. Finally, the activity is multiplied by the isotopic intensity equation (5) that was loaded into the model to receive the absolute emission rate.

$$N_A = \frac{mass}{atomic\ mass} * 6.022 * 10^{23} \quad (3)$$

$$Activity = N_A * \lambda \quad (4)$$

$$Emission_\gamma = Intensity * Activity \quad (5)$$

To validate the simulation, various isotopes were examined for the energies at which they exhibited gammas to ensure the results matched with known gamma energies. Figure 9 shows an example plot of what the gamma spec looks like for U-235 with energy in KeV on the x-axis and the emission rate on the y-axis. Highlighted is a gamma at energy 185.7 KeV which matches multiple sources as a known U-235 gamma [16], [17]. Similar results occurred with energies matching either exactly or within the given energy bin width of 4.88 KeV for other isotopes.

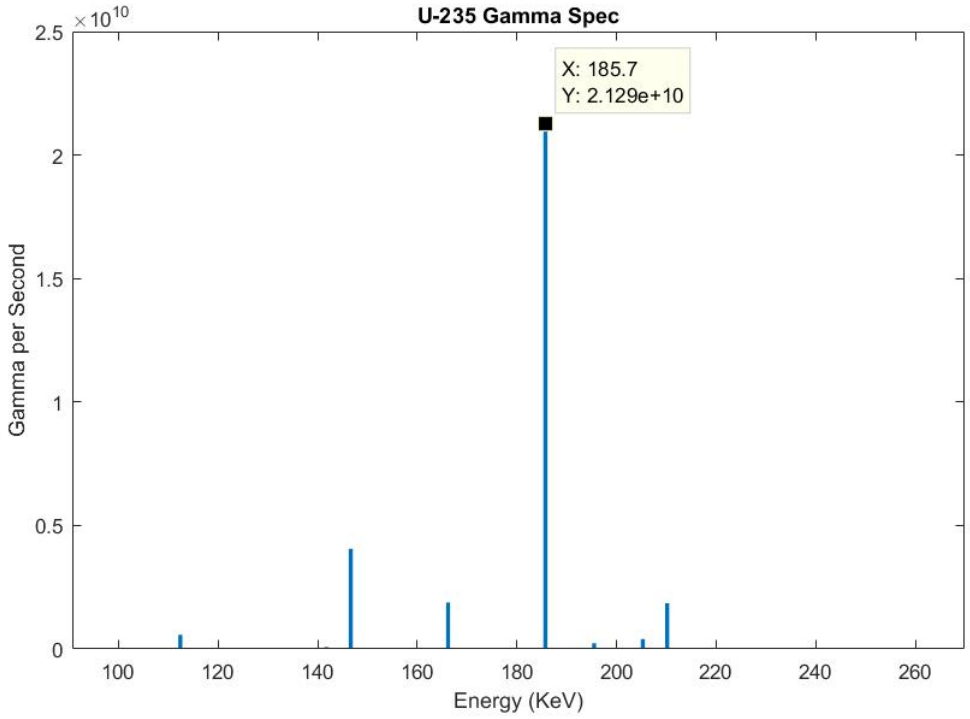

Figure 9: Example gamma emission for a 1 Ci U-235 source.

3.2 Neutron Emissions

3.2.1 Spontaneous Fission Sources

The spontaneous fission (SF) spectra can be simulated by calculations and parameters provided in the SOURCES-4C manual [18]. The average number of prompt neutrons of an actinide nuclide /k/ is $v_k(SF)$. The fraction of nuclide k that decays by spontaneous fission events are given by the SF branching fraction, F_k^{SF} , is given in equation (6) where λ_k^{SF} is the decay constant for spontaneous fission and λ_k is the overall decay constant, each for nuclide k. Thus, the average number of SF neutrons emitted per decay of nuclide k, $R_k(SF)$, is shown in equation (7). In order to compute the neutron production due to spontaneous fission per decay of nuclide /k/, the SF branching fraction and average number of neutrons per spontaneous fission are available for certain isotopes in the Origen file Origen.rev00.alphadec from SCALE-6.2.

$$F_k^{SF} = \frac{\lambda_k^{SF}}{\lambda_k} \tag{6}$$

$$R_k(SF) = F_k^{SF} v_k(SF) \tag{7}$$

The spontaneous fission neutron energy distribution given in equation (8) is approximated by a Watt's fission spectra using equation (7) and two evaluated parameters A and B. The file Origen.rev00.alphadec also contains these two parameters for 44 fissioning nuclides, 32 of which are tracked in the SSPM EChem model. All isotopes given in the file are shown in Table 1; the highlighted isotopes are ng tracked in the SSPM EChem model.

Table 1: Nuclides with spontaneous fission data and spectral parameters [15].

Isotopic Identification				
^{230}Th	^{239}U	^{240}Pu	^{244}Am	^{250}Cm
^{232}Th	^{236}Np	^{241}Pu	^{244m}Am	^{249}Bk
^{231}Pa	^{236m}Np	^{242}Pu	^{240}Cm	^{248}Cf
^{232}U	^{237}Np	^{243}Pu	^{241}Cm	^{250}Cf
^{233}U	^{238}Np	^{244}Pu	^{242}Cm	^{252}Cf
^{234}U	^{239}Np	^{240}Am	^{243}Cm	^{254}Cf
^{235}U	^{236}Pu	^{241}Am	^{244}Cm	^{253}Es
^{236}U	^{237}Pu	^{242}Am	^{245}Cm	^{254m}Es
^{237}U	^{238}Pu	^{242m}Am	^{246}Cm	^{255}Es
^{238}U	^{239}Pu	^{243}Am	^{248}Cm	

This yields a probability distribution function describing the distribution of neutron energies; thus, the total neutrons produced from spontaneous fission is the integral over all energies , equation (9). In order to calculate the multi-group spontaneous fission neutron spectrum, the Watt spectrum function is normalized according to equation (10). The resulting normalization factor is given by (11) and is shown to be dependent on the Watt spectrum parameters, A and B, for each respective isotope.

$$\chi_k^{SF}(E) = R_k(SF)e^{\frac{-E}{A}}sinh\sqrt{BE} \tag{8}$$

$$\int \chi_k^{SF}(E) = \frac{1}{4}A[-\sqrt{\pi AB}\exp\left(\frac{AB}{4}\right)\operatorname{erf}\left(\frac{A\sqrt{B}-2\sqrt{E}}{2\sqrt{A}}\right) + \sqrt{\pi AB}\exp\left(\frac{AB}{4}\right)\operatorname{erf}\left(\frac{A\sqrt{B}+2\sqrt{E}}{2\sqrt{A}}\right) - 2\left[\exp\left(2\sqrt{4BE}\right)-1\right]\exp\left(\frac{-A\sqrt{BE}+E}{A}\right)] \tag{9}$$

$$\int_0^\infty C * \chi_k^{SF}(E)dE = 1 \tag{10}$$

$$C = \frac{2}{\sqrt{\pi bA^3}}e^{-\frac{AB}{4}} \tag{11}$$

To ensure that the equations had been implemented correctly, a validation run was completed. A run was done using Origen for a single isotope, Cf-252 with an activity of 1 Ci. The second test was using the parsed information and derived equations to imitate the results of the Origen run. The Origen output is shown in Figure 10 with the neutron energy, in MeV, on the x-axis and the emission rate, neutrons per second, on the y-axis. Similarly, the output using the derived equations is shown in Figure 10. It is observed that both spectra perfectly match each other and thus it can be stated that the implemented spontaneous fission neutron spectrum calculation matches that of Origen.

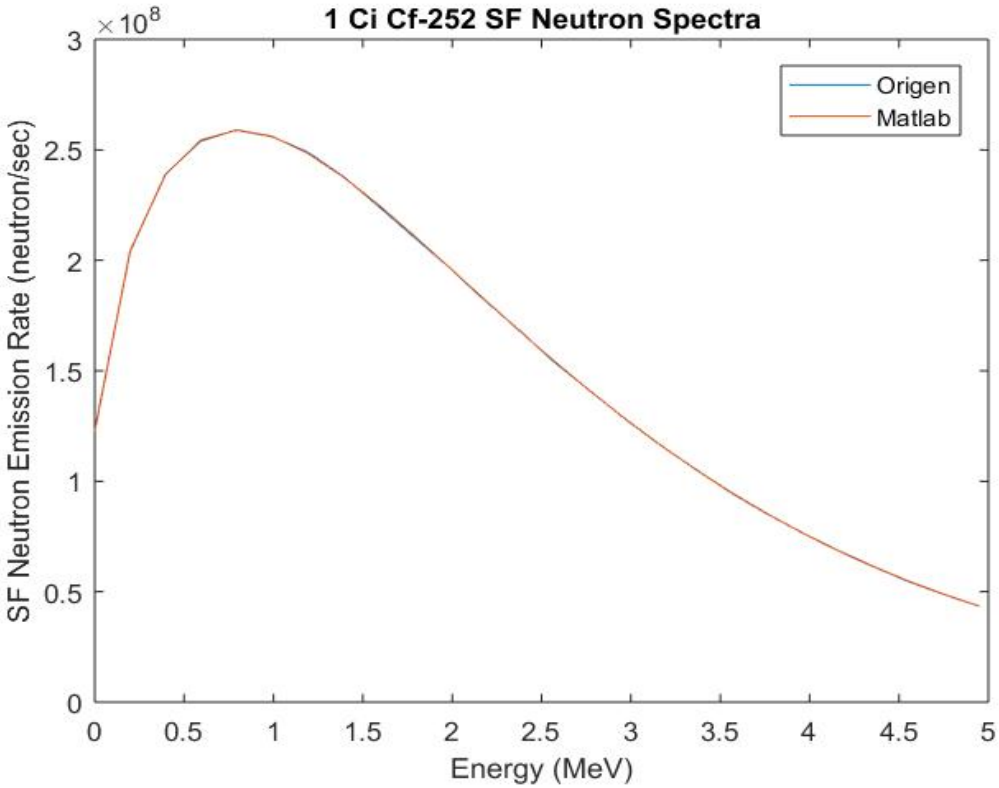

Figure 10: Origen/Sources 4-C spontaneous fission spectrum for a 1 Ci Cf-252 source.

3.2.2 (Alpha,n) Sources

The (α,n) neutron source is strongly dependent on the low-Z content of the medium containing the alpha-emitting nuclides and requires modeling the slowing down of the alpha particles and the probability of neutron production as the α particle, at energy E_a, slows down [6],[18]. The calculation assumes (1) a homogeneous mixture in which the alpha-emitting nuclides are uniformly mixed with the target nuclides and that (2) the dimensions of the target are much larger than the range of the alpha particles. Thus, all alpha particles are stopped within the mixture. The slowing and stopping of alpha particles is described by the material's stopping power equation (12) which yields the particles energy loss per length traveled. Similarly, the distance traveled, L, in slowing down equation (13) is calculated by taking the integral between the original and new alpha particle energy.

$$\Delta E_\alpha = E_\alpha - E'_\alpha \tag{12}$$

$$L = \int_{E_\alpha}^{E'_\alpha} \frac{1}{\frac{dE}{dx}} dE \tag{13}$$

Next, the probability that a traveling alpha will induce a reaction producing a neutron is calculated. The probability of an (α,n) interaction with nuclide /i/ by an alpha particle at energy E traveling from x to x+dx is shown in equation (14). Where N is the atom density, $\sigma_i(E)$ is the energy dependent cross section, and $\frac{dE}{dx}$ is the stopping power. It is dependent upon the atom density of the nuclide i and the corresponding microscopic cross section for nuclide i. Thus, the probability of

interaction, when taking into account the changing energy from the slowing down of the alpha particle is calculated by equation (15).

$$N_i \sigma_i dx = \frac{N_i \sigma_i(E)}{(\frac{dE}{dx})} \tag{14}$$

$$p_i(E_\alpha \rightarrow E'_\alpha) = \int_{E_\alpha}^{E'_\alpha} \frac{N_i \sigma_i(E)}{(\frac{dE}{dx})} dE \tag{15}$$

To calculate the probability of an interaction occurring before the alpha particle has stopped within the medium, given in equation (16), the energy is integrated from zero to the original alpha energy. This function is often referred to as the thick-target neutron production function.

$$P_i(E_\alpha) = \int_0^{E_\alpha} \frac{N_i \sigma_i(E)}{\left(-\frac{dE}{dx}\right)} dE \tag{16}$$

Introducing the stopping cross section equation (17) can further simply the previous function. The stopping cross section is defined by the stopping power and the total atom density of the medium consisting of j constituents, shown in equation (18). Now the thick-target neutron production function is expressed in terms of the stopping cross section, in equation (19).

$$\varepsilon(E) = -\frac{1}{N}\frac{dE}{dx} \tag{17}$$

$$\varepsilon(E) \cong \frac{1}{N}\sum_{j=1}^{J} N_j \varepsilon_j(E) \quad where \;\; N = \sum_{j=1}^{J} N_j \tag{18}$$

$$P_i(E_\alpha) = \frac{N_i}{N}\int_0^{E_\alpha} \frac{\sigma_i(E)}{\varepsilon(E)} dE \tag{19}$$

Next, one must consider the rate at which nuclides within the material will decay via alpha emission. This fraction given in equation (20) may occur with the emission of one of L possible alpha energies. The intensity, $f_{k\ell}^{\alpha}$, is the fraction of all decays of nuclide k resulting in an alpha particle of energy E_l. Thus, the fraction of nuclide k decays resulting in a reaction in a medium containing i nuclides is given in equation (21).

$$F_k^{\alpha} = \sum_{\ell=1}^{L} f_{k\ell}^{\alpha} \tag{20}$$

$$R_k(\alpha, n) = \sum_{\ell=1}^{L} f_{k\ell}^{\alpha} \sum_{i=1}^{I} P_i(E_\ell) \tag{21}$$

These calculations are conducted assuming an isotropic neutron angular distribution in the center-of-mass (COM) system. An example of such a system for an (α,n) reaction is shown in Figure 11.

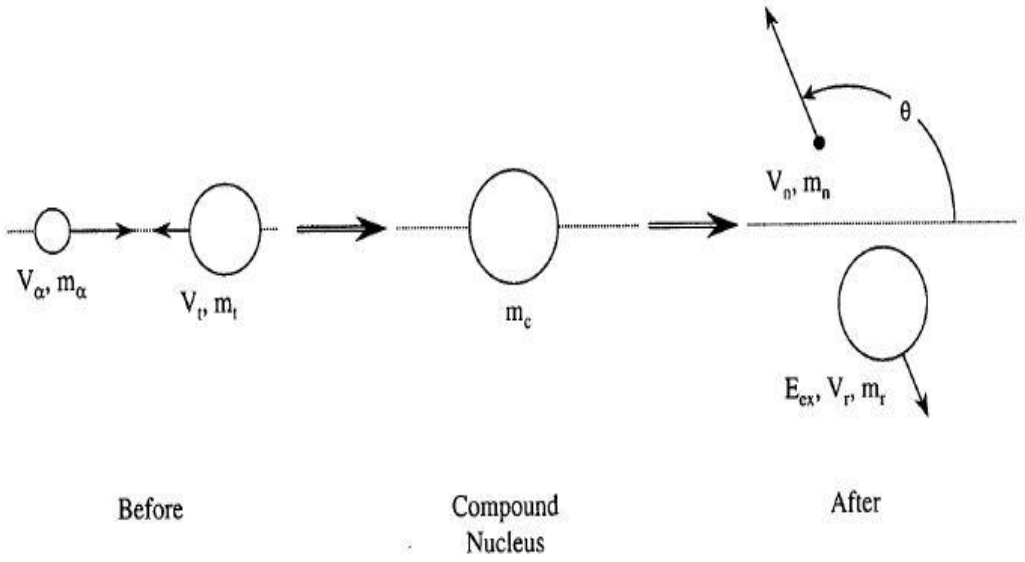

Figure 11: An (α,n) reaction in the COM system [18].

Taking into account the conservation of momentum, the velocity of the COM is dependent on the alpha particle velocity in a laboratory setting along with the alpha particle and target nuclide mass. Subtracting this velocity from the particle velocities yields equations (22) and (23), which are the alpha particle and target nuclide velocities in the COM system. Each are dependent on a variation of the alpha and target masses, m_α and m_t along with the alpha particle velocity in a laboratory setting, v_α^{lab}.

$$v_\alpha^{CM} = v_\alpha^{lab}\left(\frac{m_t}{m_\alpha + m_t}\right) \tag{22}$$

$$v_t^{CM} = -v_\alpha^{lab}\left(\frac{m_\alpha}{m_\alpha + m_t}\right) \tag{23}$$

Observing the conservation of energy in the COM system, the neutron kinetic energy given in equation (24) is dependent on five variables: the Q-value of the reaction; the excitation level of the recoil nucleus E_{ex}; and the kinetic energies of the alpha particle KE_α, the target nucleus KE_t, and the recoil nucleus KE_r. The kinetic energy of the recoil nucleus, along with the relationship between the kinetic energy of the alpha and target nucleus, are shown in equations (25) and (26).

$$KE_n = (Q - E_{ex}) + KE_\alpha + KE_t - KE_r \tag{24}$$

$$KE_r = \frac{1}{2}m_r v_r^2 = \frac{1}{2}\frac{m_n^2}{m_r}v_r^2 = KE_n\left(\frac{m_n}{m_r}\right) \tag{25}$$

$$KE_\alpha + KE_t = E_\alpha^{lab}\left(\frac{m_t}{m_\alpha+m_t}\right) \tag{26}$$

Substituting equations (25) and (26) into equation (24) and solving for the kinetic energy of the neutron yields equation (27). The variable Q_m is a simplification made and is equal to the first term in equation (24), the Q-value minus the excitation energy.

$$KE_n = Q_m\left(\frac{m_r}{m_r+m_n}\right) + E_\alpha\left(\frac{m_t}{m_\alpha+m_t}\right)\left(\frac{m_r}{m_r+m_t}\right) \tag{27}$$

Using the definition of kinetic energy, the neutron velocity in the COM system is represented by equation (28). This can be converted to the neutron velocity in the laboratory system according to equation (29) by adding the velocity of the COM.

$$v_n = \pm\sqrt{\frac{Q_m}{m_n}\left(\frac{m_r}{m_r+m_n}\right) + \frac{E_\alpha}{m_n}\left(\frac{m_t}{m_\alpha+m_t}\right)\left(\frac{m_r}{m_r+m_t}\right)} \tag{28}$$

$$v^{lab} = \left(\frac{m_\alpha}{m_\alpha+m_t}\right)\sqrt{\frac{2E_\alpha}{m_\alpha}} \pm \sqrt{\frac{Q_m}{m_n}\left(\frac{m_r}{m_r+m_n}\right) + \frac{E_\alpha}{m_n}\left(\frac{m_t}{m_\alpha+m_t}\right)\left(\frac{m_r}{m_r+m_t}\right)} \tag{29}$$

Using the neutron velocity in the laboratory frame and the definition of kinetic energy, it is possible to determine the neutron energy given in equation (30) from an incident alpha particle of energy E_α that generates a product nuclei of level m. This relates the maximum and minimum permissible neutron energies.

$$E_{n,m}^{\pm} = \left(\sqrt{E_\alpha a_1}\left(\frac{1}{1+a_1}\right) \pm \sqrt{\frac{Q_m}{m_n}\left(\frac{1}{1+a_3}\right) + E_\alpha\left(\frac{a_2}{1+a_2}\right)\left(\frac{1}{1+a_3}\right)}\right)^2 \quad (30)$$

$Where$: $a_1 = \frac{m_n}{m_\alpha}$, $a_2 = \frac{m_t}{m_\alpha}$, $a_3 = \frac{m_n}{m_r}$

The fraction of target i product level m reactions of source k alpha particles occurring in the energy group g is given by equation (31). The variable $P_i(E_l)$, defined by equation (32), is the discrete form of equation (19).

$$H_{i,k}^{l}(m) = \frac{P_i(E_{l+1}) - P_i(E_l)}{P_i(E_\alpha)} \quad (31)$$

$$P_i(E_l) = \frac{N_i}{N}\sum_{g=1}^{G-1}\frac{1}{2}\left[\frac{\sigma_i^{g+1}}{\varepsilon^{g+1}} + \frac{\sigma_i^{g}}{\varepsilon^{g}}\right](E^{g+1} - E^{g}) \quad (32)$$

The branching fraction of alpha particles at energy E_α reacting with target nuclide i and producing product level m is interpolated by equation (33) where f_i is the probability of a recoil nucleus being in a certain excitation state. Therefore, the fraction of alpha particles at energy E_α with target nuclide i and resulting in product level m reactions occurring in the alpha particle energy group g is the product of equations (31) and (33), yielding equation (34). Assuming that all neutrons are isotropically emitted from the compound nucleus, they will evenly contribute to all energy groups, defined by equation (30). Thus, the contribution per decay of source nuclide k to neutron energy group g is given by equation (35).

$$S_{i,k}(m) = f_i(m, m' - 1) + (f_i(m, m') - f_i(m, m' - 1)) \frac{E_\alpha - E(m' - 1)}{E(m') - E(m' - 1)} \quad (33)$$

$$F_{i,k}^{l}(m) = S_{i,k}(m) H_{i,k}^{l}(m) \quad (34)$$

$$\chi_k^{(\alpha,n)}(E_g) = R_k(\alpha, n) F_{i,k}^{l}(m) \frac{E_{g+1} - E_g}{E_{n,m}^{+} - E_{n,m}^{-}} \quad (35)$$

Origen contains four files, listed in Table 2, regarding (α,n) reactions where all the information was parsed and then stored in .mat files so that it could be loaded into the SSPM EChem model. In total, information was parsed for 45 isotopes in relation to the file ALPHDEC, which provides alpha energies and yields. Information regarding stopping power and cross section data was parsed from the respective files for six target isotopes that the alpha particles will interact with to produce neutrons.

Table 2: Neutron source data libraries [6].

File Name	Description
ALPHDEC	Neutron source decay data
STCOEFF	Stopping power coefficients
ALPHYLD	Target (α,n) product level branching
ALPHAXS	Target (α,n) cross section

To ensure that the equations had been implemented correctly, one validation run was completed. Origen was used to run a single reaction Pu238(α,n) O18 each with a mass of 100 grams. The second test was using the parsed information and derived equations to imitate the results of the Origen run. Both emission spectrum should yield exactly the same results. The Origen output is shown in Figure 12 with the neutron energy, in MeV, on the x-axis and the emission rate, neutrons per second, on the y-axis. Similarly, the output using the derived equations is shown in Figure 12. It is observed that both spectra match each other in most regards with slight differences in a few energy bins. This difference is minimal and suggests the (α,n) code is not yet suitable to give completely accurate results but is close enough to give approximations.

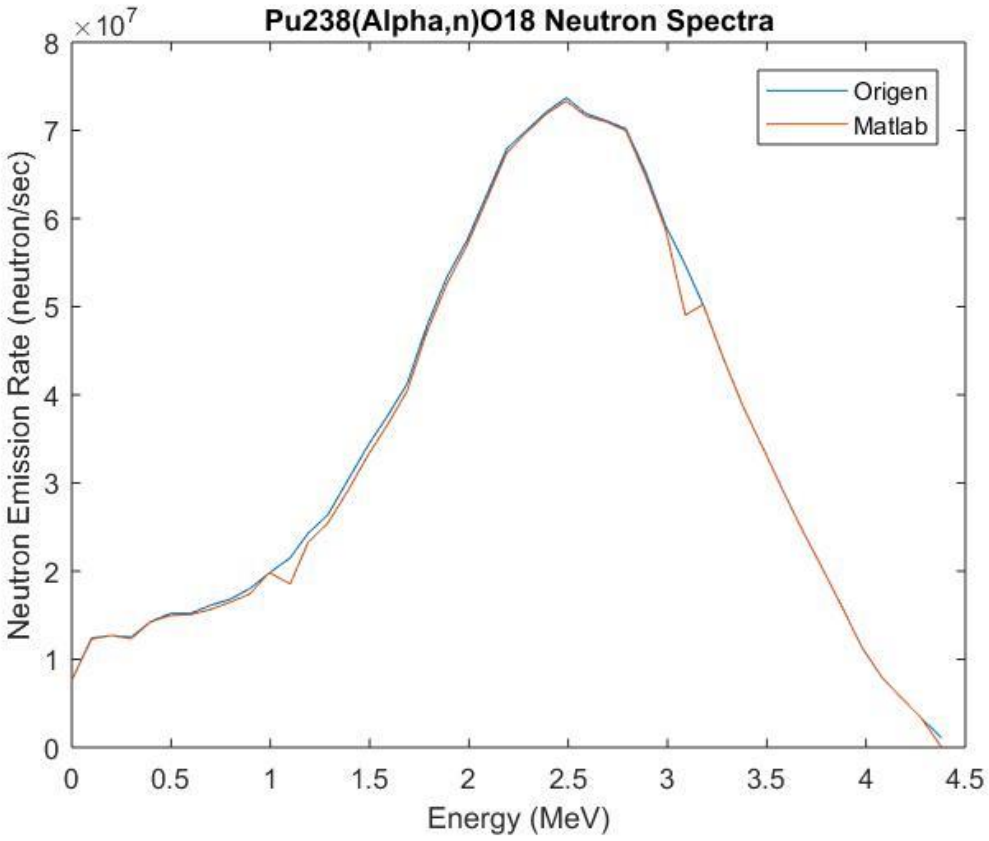

Figure 12: Origen/Sources 4-C (α,n) spectrum for Pu238(a,n)O18.

3.2.3 Total Neutron Sources

The total neutron spectra were calculated by adding the spontaneous fission and (α,n) sources. A simulation was performed at the electrorefiner to determine contribution of each source to the total counts. Figure 13 shows this contribution to the neutron emission rate as a function of energy. The spontaneous fission source aligns closely with that of the total counts, while the (α,n) drops significantly above 1.5 MeV. In all the spontaneous fission accounts for roughly 80% of the total neutron count, while the (α,n) source accounts for the remaining 20%. This does vary slightly, regarding fuel within the SSPM EChem model, depending on the burnup and enrichment of the fuel but nonetheless, shows that the (α,n) contribution is non-negligible.

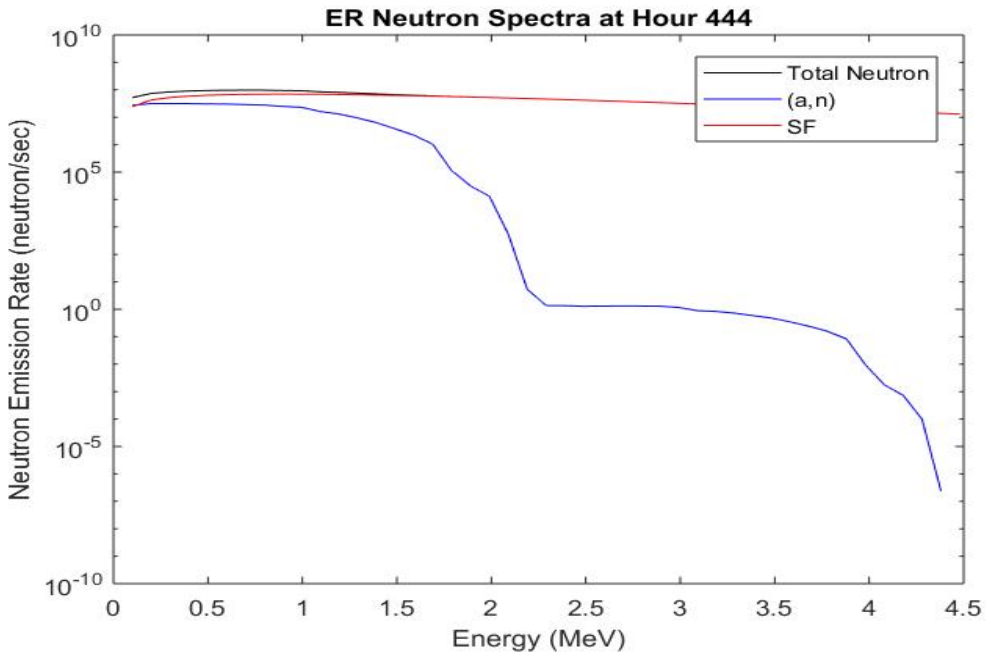

Figure 13: Contribution to the total neutron spectra at the electrorefiner.

Table 3 lists the exact contribution values wherein the total (α,n) source term and primary isotopic contributors for three burnup values (33, 45, and 60 GWd/MTHM), each with three different enrichment values. All runs were performed using a cooling time of five years and evaluated at the batch run hour 444. It is seen that the overall contribution centers around 20% with certain cases deviating by +/- 8% of that center value.

A break down shows how maintaining a constant burnup while fluctuating the enrichment effects the overall (α,n) emission rate, its contribution to the total neutron counts, and four isotopic contributions to the (α,n) emission rate. As the enrichment is increased, the overall (α,n) contribution to total counts increases. Holding enrichment constant while changing the burnup demonstrates as burnup is increased, the contribution to the total counts decreases. In both scenarios, there is an inverse relationship between the contribution from ^{238}Pu and ^{244}Cm to the (α,n) emission rate. For the case of constant burn-up, as enrichment increases so does the contribution from ^{38}Pu where the contribution from ^{244}Cm then decreases. For the case of constant enrichment, as burnup increases so does the relative contribution from ^{244}Cm where the relative contribution from ^{238}Pu then decreases. This corresponds to the fluctuation in the share of neutrons between spontaneous fission and the (α,n) reactions.

Next, plutonium and curium isotopes were broken down to determine two things. First, what isotopes are the main contributors to the (α,n) spectrum and second, is an (α,n) calculation a good accountancy measurement in terms of plutonium build up. Regarding the first case, it appears that for the fuel tested, ^{38}Pu and ^{244}Cm make up on average 70-80% of all (α,n) counts. The majority of (α,n) neutrons are produced from ^{244}Cm decay. Meaning this is a good indicator of both spontaneous fission and (α,n) neutrons. The second inquiry of plutonium buildup is also intriguing as it is the second highest neutron contributor.

Table 3: Summary of (a,n) results showing burnup/enrichment mixtures.

Burn-up (GWd/MTHM)	Enrichment (%)	Total(a,n) Emission Rate (n/s)	Percent Contribution to Total Counts (%)	Percent Isotopic Contribution to (α,n) (%)			
				Pu-238	Pu-239	Pu-240	Cm-244
33	2.60	3.404E8	19.73	31.29	1.62	2.84	50.57
33	3.30	2.658E8	23.85	36.67	2.20	3.34	41.01
33	4.00	2.174E8	28.70	40.80	2.82	3.76	33.11
45	3.30	6.560E8	17.12	27.88	0.90	1.69	60.91
45	4.00	5.276E8	18.81	32.97	1.18	1.99	53.24
45	4.70	4.367E8	22.08	37.47	1.50	2.27	46.16
60	4.03	1.229E9	14.53	24.08	0.48	1.00	69.13
60	4.73	1.020E9	16.44	28.44	0.63	1.16	63.31
60	5.43	8.587E8	18.01	32.60	0.78	1.33	57.57

CHAPTER 4: RESULTS AND ANALYSIS

Both radiation signatures, gamma emissions and total neutron emissions were modeled and implemented in the SSPM EChem model. The spontaneous fission and (α,n) simulations were combined to give the total neutron spectra. Details surrounding the runs are as follows:

- The chosen burnup was 33 GWd/MTHM.
- The fuel was enriched by 2.6%.
- The discharge time of the fuel was 5 years.
- A total of 600 hours of operational time was simulated.
- Diversion scenarios occurred between hours 300-500.
- Direct diversion was chosen as the diversion method.

These criteria were used for a total of eight locations, all within MBA2, and included runs capturing normal conditions as well as diversion scenarios ranging from 10-50% material diversion. The diversion scenarios modeled here are notional to demonstrate the concept of changing radiation signatures and online monitoring. Figure 14 showcases the mass change over time at the electrorefiner under normal conditions. This is to give visual representation of how the electrochemical cycle works in a batch format with mass increased during a six hour batch run and mass decreased during the eighteen hours between batches. To ensure a proper analysis was done, each radiation signature was taken at batch hour 444, ensuring that fuel is present and the effect of each diversion scenario will be seen. An examination of all runs for each radiation signatures for three out of the nine locations; the electrofiner salt, the metal processing unit, and the UTRU drawdown is given.

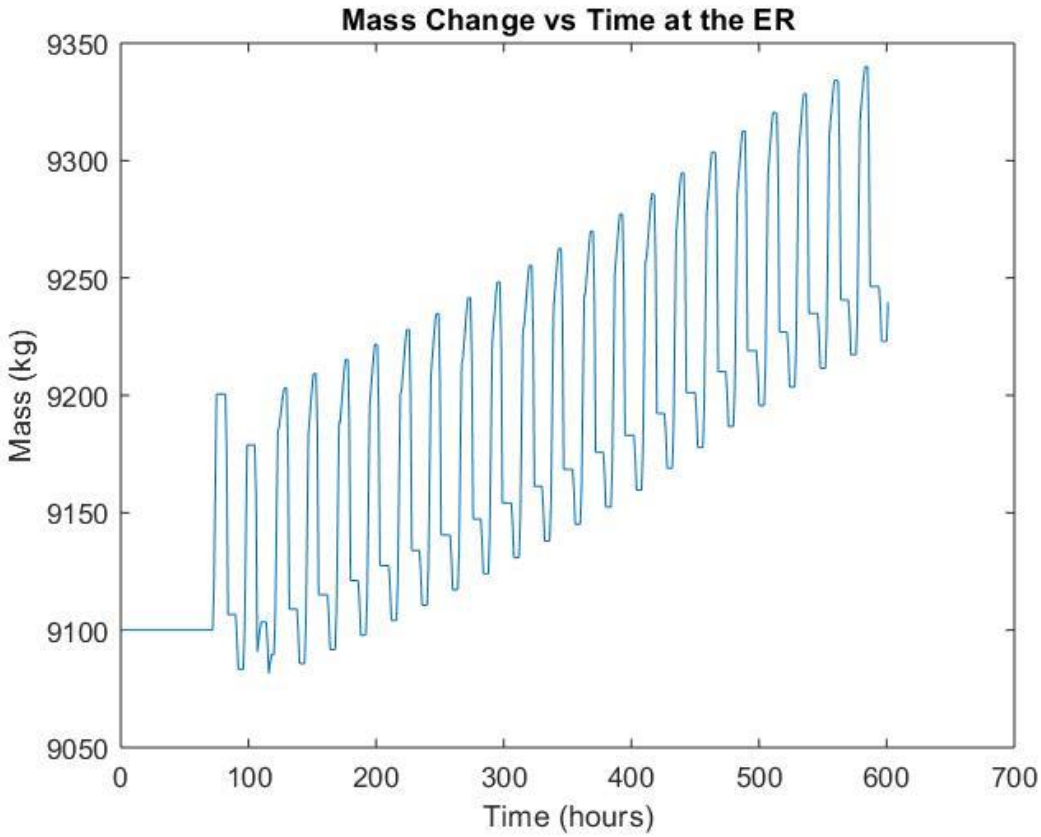

Figure 14: Mass change as a function of time at the ER.

4.1 Electrorefiner Spectra

The first location examined was the electrorefiner; it is the main unit that drives the electrochemical process and has the largest variety of isotopes at a single location. The gamma simulation, seen in Figure 15, yielded results where certain gamma rays are observable with the emission rate decreasing in accordance with material quantity (i.e. the legend represents the normal scenario and each number corresponds to the percent mass diversion). Figure 16 showcases typical results from the total neutron simulation measurements. In the electrorefiner, actinides are actively in the salt and thus yield a spectrum under normal conditions. As material is diverted away, the magnitude of the emission rates decreases.

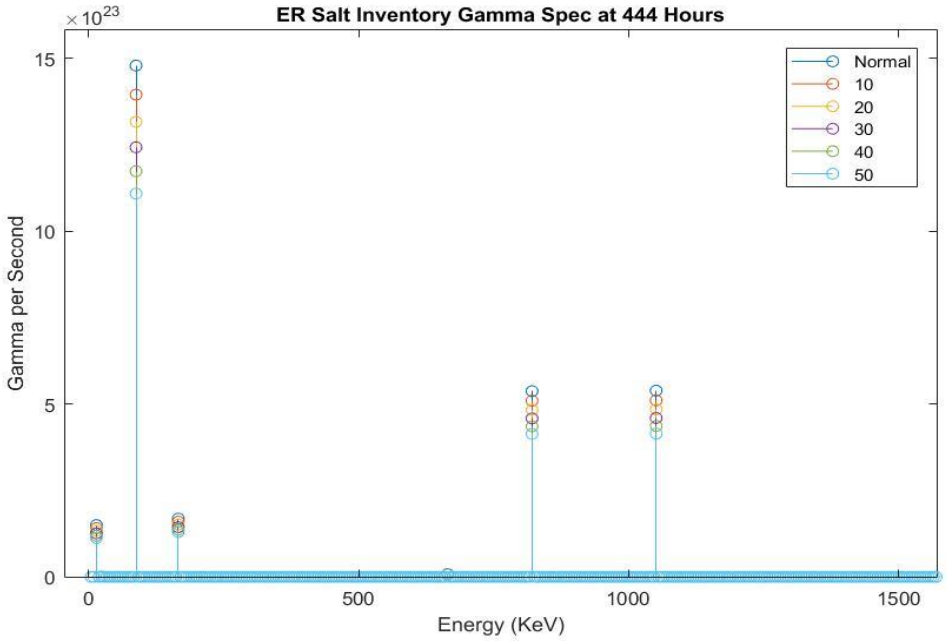

Figure 15: Gamma spectra of the ER salt for different diversion scenarios.

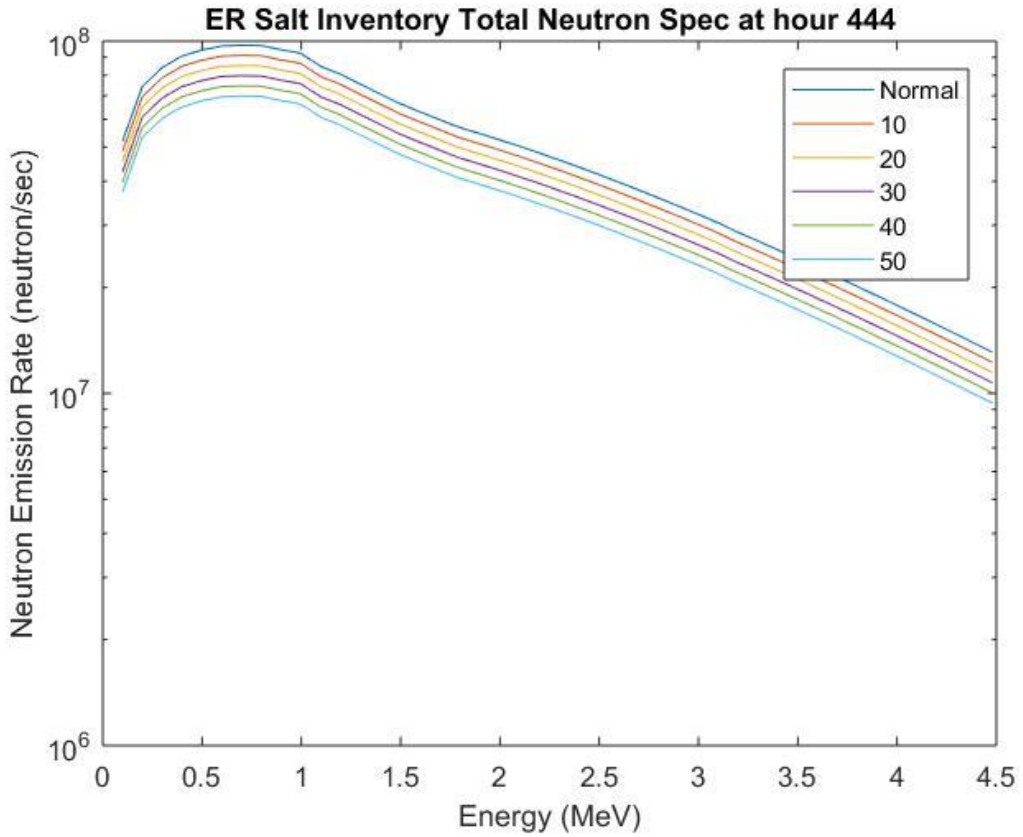

Figure 16: Total neutron spectra of the ER salt for different diversion scenarios.

4.2 Metal Processing Spectra

The second location is the metal processing unit. Although this is not one of the more high-profile areas when it comes to proliferation risk, it is still necessary to be able to properly track material moving through it. Regarding gamma emissions, seen in Figure 17, the intuitive order of each scenario does not yield normal conditions as having the highest magnitude, with diversion scenarios subsequently decreasing with increasing material diversion. Instead, the magnitude of each scenario is more sporadic.

Similar features are seen in Figure 18, which shows the total neutron spectra for the metal processing unit. Again, the order is influenced by the inner workings of the SSPM EChem model, but one is able to distinguish the magnitude of each emission between that of each scenario. A highlight from this location is the ability for the model to differentiate when the magnitude of the spectra is of such low value. A portion of this stems from the mathematical computations within Simulink where once a notional diversion scenario occurs the material quantity is relatively zero and the resulting magnitude comes from calculation rounding. What is to be taken away is that even with this mathematical property, differentiation between normal and off-normal conditions still occurs.

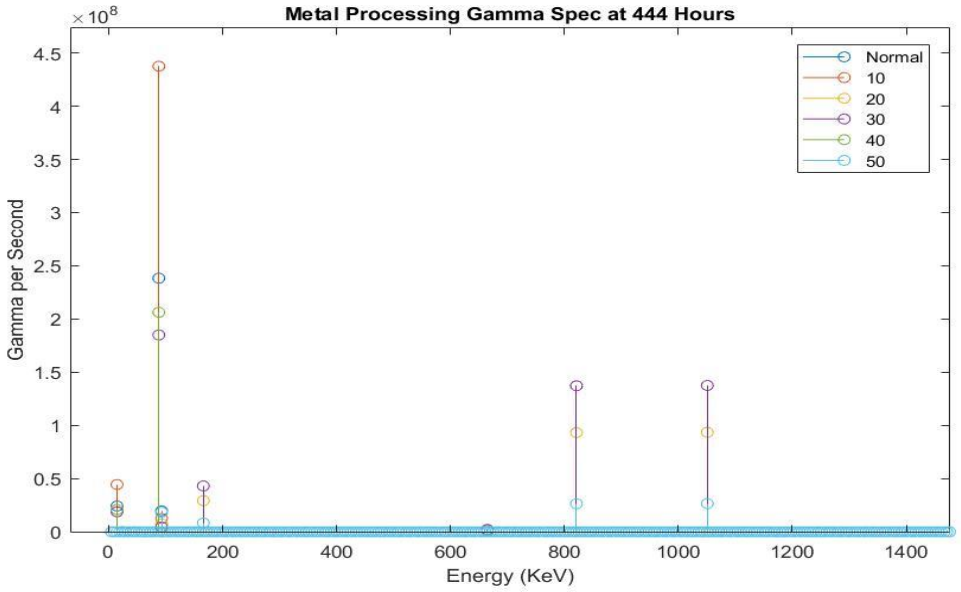

Figure 17: Gamma spectra at the metal processing unit for different diversion scenarios.

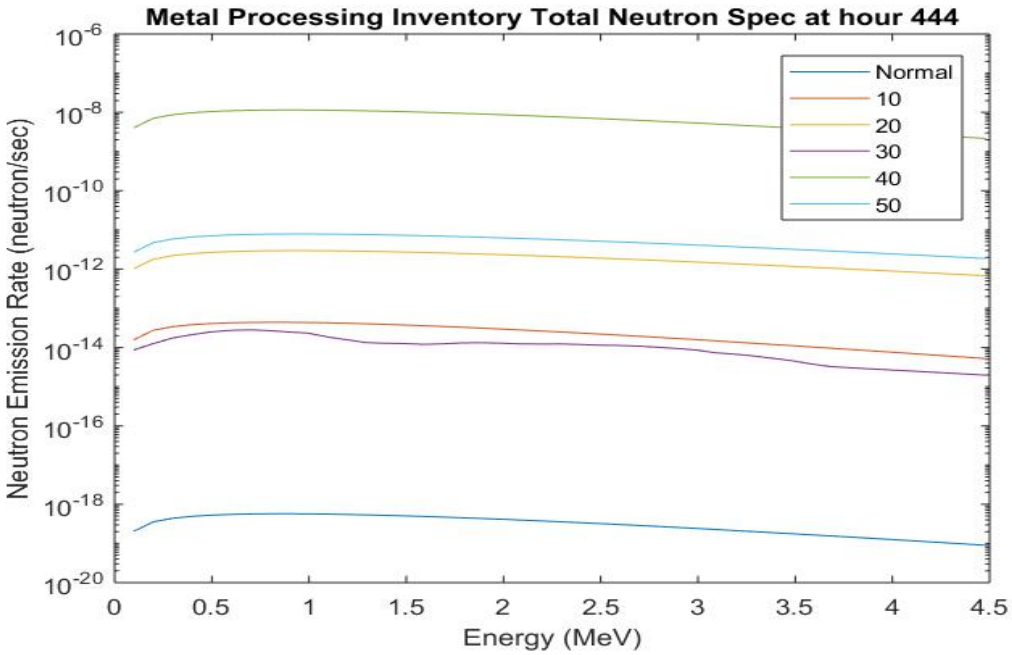

Figure 18: Total neutron spectra at the metal processing unit for different diversion scenarios.

4.3 Drawdown Spectra

The last area that will be highlighted is the drawdown unit that feeds into the salt purification process. Here, the gamma emissions, seen in Figure 19, are relatively low in magnitude when compared to other locations. Thus, when undergoing material diversion, it is seen that enough material is siphoned, even under only 10% diversion, that the effect yields no gamma spectrum. Therefore, each peak observed is only from the normal condition scenario. All subsequent diversion scenarios yield zero gamma rays.

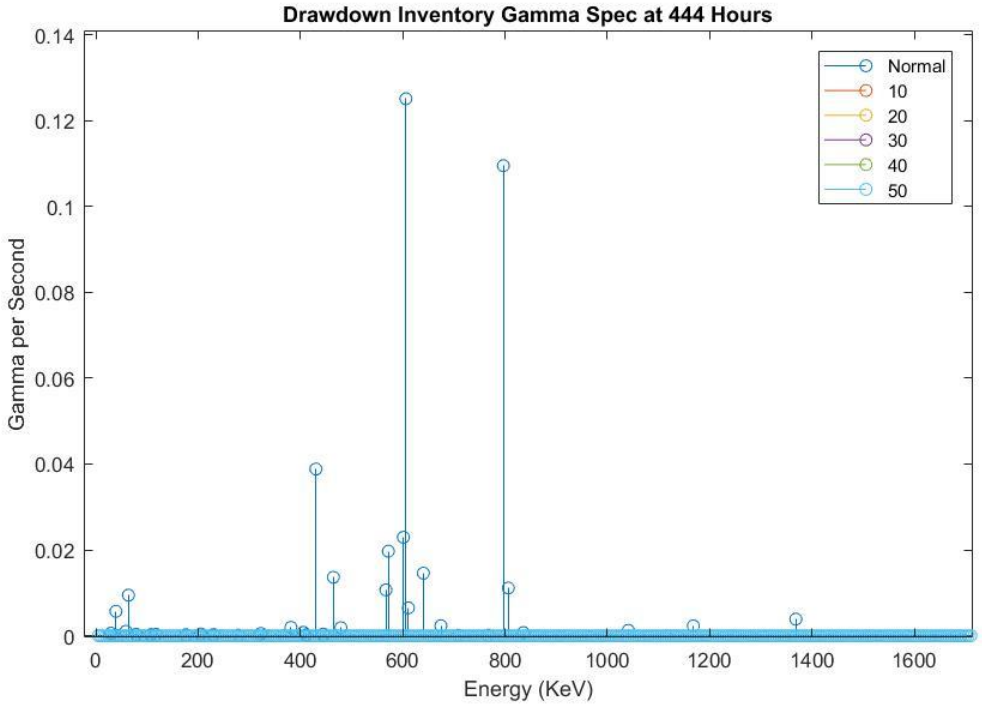

Figure 19: Gamma spectra at the drawdown unit for different diversion scenarios.

The total neutron spectrum, shown in Figure 20, is meant to showcase how the model is able to differentiate operating conditions between small magnitudes. At this point in the process, the actinide quantity is relatively low and thus shouldn't yield a high magnitude spectrum. Under normal conditions, a spectrum with a small emission rate is observable. It should be noted that this is due to the mathematical rounding performed by Simulink. Once material has been diverted there is no longer a substantial actinide quantity to yield results allowing for normal and off-normal condition differentiation.

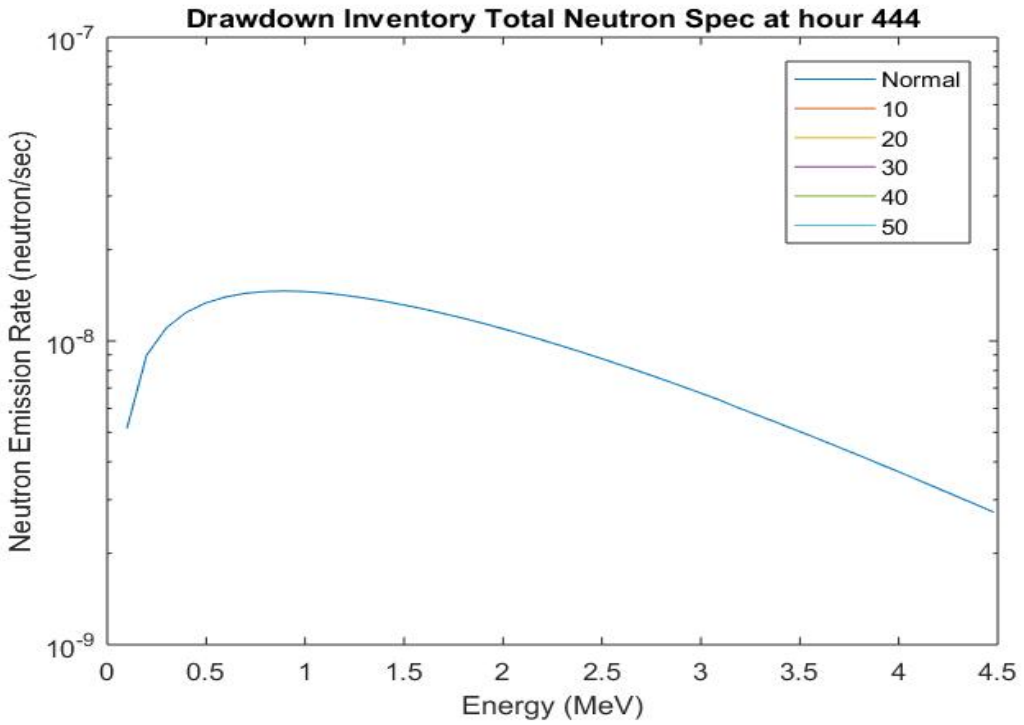

Figure 20: Total neutron spectra at the drawdown unit for different diversion scenarios.

4.4 Diversion Ratios

Analysis of the relationship between the normal and diversion scenarios shown was also done to determine if the decrease in the observed emissions were proportional to the mass diversion. For this the ratio between normal and diversion scenarios were taken and plotted against amount diverted. Since each diversion yielded emissions of zero for both signatures at the drawdown unit, this analysis will be presented only for the electrorefiner and metal processing units. Figure 21 shows the corresponding relationship between the drop-in count rate to diversion for the electrorefiner for both signatures. It is seen that for both signatures the relationship is nearly linear. Thus, there does appear to be some proportionality between the decrease in the observed emission rates and the mass diversion but further investigation is necessary to determine if this same relationship holds for different diversion scenarios and fuel configurations.

Figure 22 shows the corresponding relationship between the drop-in count rate to diversion for the metal processing unit for both signatures. It is seen that for both signatures there appears to be no discernable relationship. This can be attributed to the inner working of the EChem model but further analysis must be done to soundly provide a reason for this phenomenon.

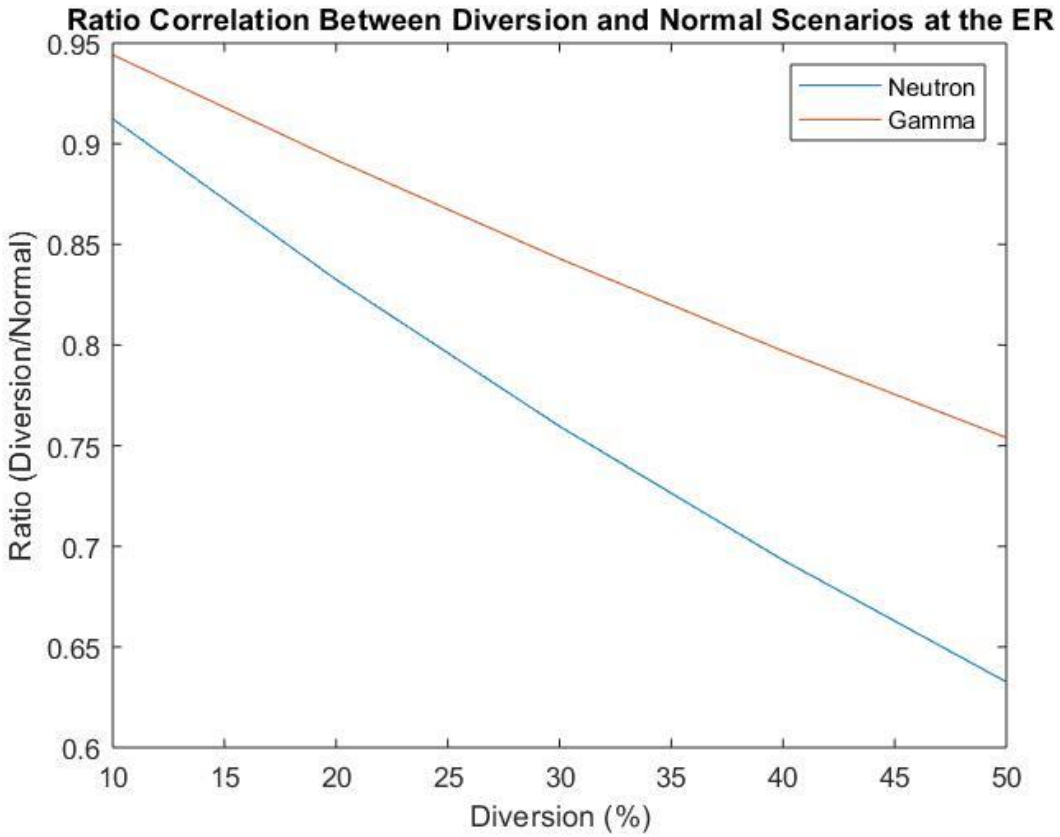

Figure 21: Ratio correlation between diversion scenarios at the ER unit for gamma and total neutron emissions.

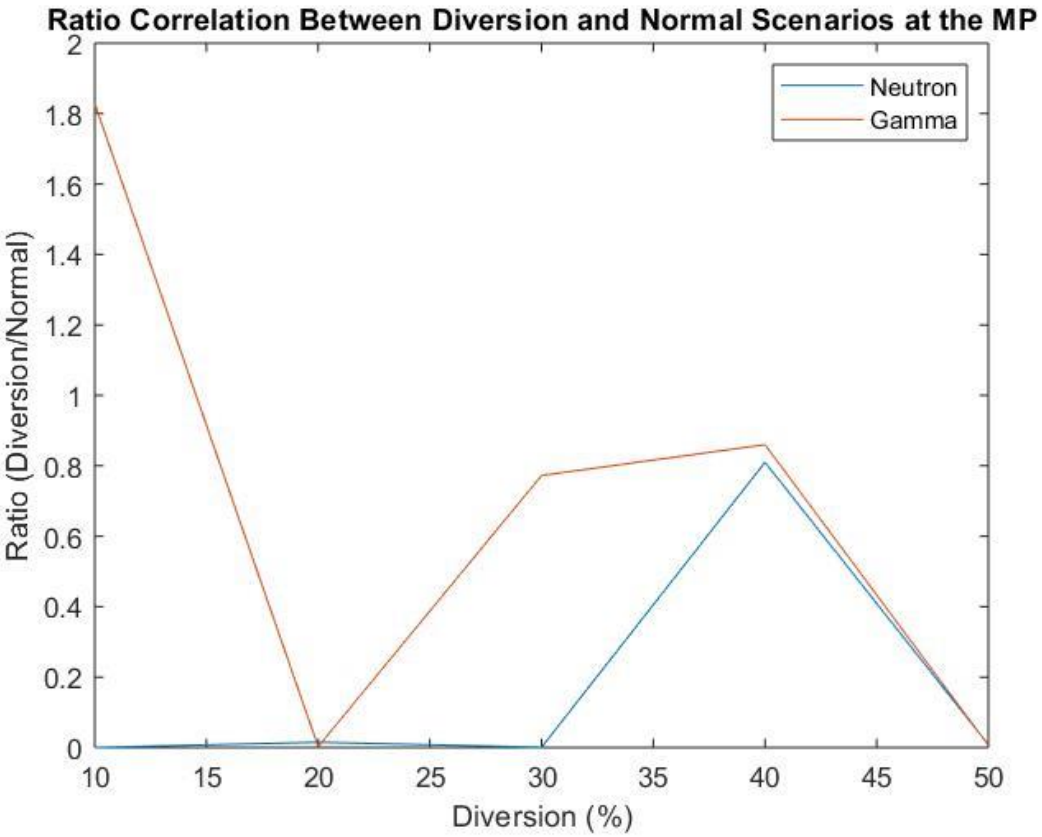

Figure 22: Ratio correlation between diversion scenarios at the metal processing unit for gamma and total neutron emissions.

CHAPTER 5: CONCLUSIONS

The simulations developed in support of this work have shown that gamma and total neutron emissions can be applied as a safeguards measurement technique in the SSPM EChem model. While there appear to be some model peculiarities, mainly stemming from the mathematical rounding performed by Simulink, each technique is able to differentiate between normal and off-normal conditions for multiple locations throughout the pyroprocessig cycle. The gamma responses clearly show unique energy peaks and for the most part yield emission magnitudes in accordance with the amount of material at the specific location. Only under conditions where the amount of gamma emitting material is scarce, does the emission magnitude order vary for the given scenarios. In actual gamma spectra, however, one would not see distinct peaks and thus further study must be done regarding more realistic gamma spectra. Similarly, the neutron responses often indicate abnormalities when concerned with actinide concentration. The neutron simulation properly simulates the emission rates in expected order, given the performed scenarios, except when the material quantity is low. Under these circumstances, mathematical rounding can lead to spectrum of a various order but still allows for proper quantification and differentiation between normal and off-normal conditions. It is due to these specific occurrences that the techniques described should be performed simultaneously to ensure proper material quantification. The diversion scenarios modeled here were notional and performed simply to demonstrate the concept of using gamma and neutron spectra as part of a safeguards approach.

5.1 Future Work

The next step is the advancement of each measurement technique application to simulate actual detector response. The current implementation only deals with

source term emission rate. While this is beneficial as a first stage deployment tool for material accountancy, the reality outside the realm of simple emission rate is far more complex. It will also aid in future work in regards to diversion scenarios that could be tested to enhance the safeguards aspects of the model. Additional work would involve the development of additional signatures to be added to the model to better track individual isotopes and monitor various process throughout the facility.

LIST OF REFERENCES

[1] M. F. Simpson and J. D. Law, “Nuclear Fuel Reprocessing,” *Inl/Ext-10-17753*, no. February, pp. 121–126, 2010.
[2] H. Lee *et al.*, “Current status of pyroprocessing development at KAERI,” *Sci. Technol. Nucl. Install.*, vol. 2013, 2013.
[3] B. B. Cipiti, F. A. Durán, B. Key, Y. Liu, and I. Lozano, “Modeling and Design of Integrated Safeguards and Security for an Electrochemical Reprocessing Facility,” no. October, 2012.
[4] T. Inoue, T. Koyama, and Y. Arai, “State of the art of pyroprocessing technology in Japan,” *Energy Procedia*, vol. 7, pp. 405–413, 2011.
[5] H. Lee, “Pyroprocessing Technology Development at KAERI Integrated Pyroprocessing in PRIDE,” 2010.
[6] B. T. Rearden and M. A. Jessee, *SCALE Code System*, no. April. 2016.
[7] J. H. Yoo, C. S. Seo, E. H. Kim, and H. S. Lee, “A conceptual study of pyroprocessing for recovering actinides from spent oxide fuels,” *Nucl. Eng. Technol.*, vol. 40, no. 7, pp. 581–592, 2008.
[8] Y. Z. Cho, G. H. Park, H. C. Yang, D. S. Han, H. S. Lee, and I. T. Kim, “Minimization of eutectic salt waste from pyroprocessing by oxidative precipitation of lanthanides,” *J. Nucl. Sci. Technol.*, vol. 46, no. 10, pp. 1004–1011, 2009.
[9] B. B. Cipiti, “OPTIMIZING NEAR REAL TIME ACCOUNTABILITY FOR REPROCESSING * Benjamin B. Cipiti Sandia National Laboratories P.O. Box 5800, MS 0747, Albuquerque, NM 87185-0747.”
[10] B. S. Tomar, “Gamma ray spectrometry,” *Nucl. Anal. Tech.*, no. September, pp. 162–170, 2002.
[11] W. L. Dunn and D. S. McGregor, “Gamma-ray detectors,” *Handb. Part. Detect. Imaging*, pp. 413–451, 2012.
[12] P. De Felice, “Workshop on Understanding and Evaluating Radioanalytical Measurement Uncertainty,” no. November, 2007.
[13] R. J. Holmes, “Chapter 3 gamma-ray and neutron sources r.j. holmes.”
[14] T. For, S. Dorothy, and R. Mcelroy, “Comparison Of Neutron Coincidence And Multiplicity Counting,” no. Figure 1, pp. 1–6.
[15] J. Sprinkle, “Total Neutron Counting Instruments and

Applications,” *12th Int. Conf. Sci. Inf.*, vol. 1, no. July, pp. 435–455, 2009.
[16] T. D. Reilly, “1 . Principal NDA Gamma-Ray Signatures,” *October*, pp. 1–19.
[17] I. Parent, “8th Edition of the Table of Isotopes : 1998 Update Table 2 . Principal Gamma-Rays from Isotopes with Half-lives > 1 . 0 h An energy-ordered list of principal γ rays from nuclei whose parent or grandparent half-life exceeds 1 . 0 h is given in Table 2 . Th,” pp. 107–128, 1998.
[18] C. J. Turner, “Los Alamos,” vol. 836, pp. 0–10, 2002.

APPENDIX

Appendix A: Gamma Plots

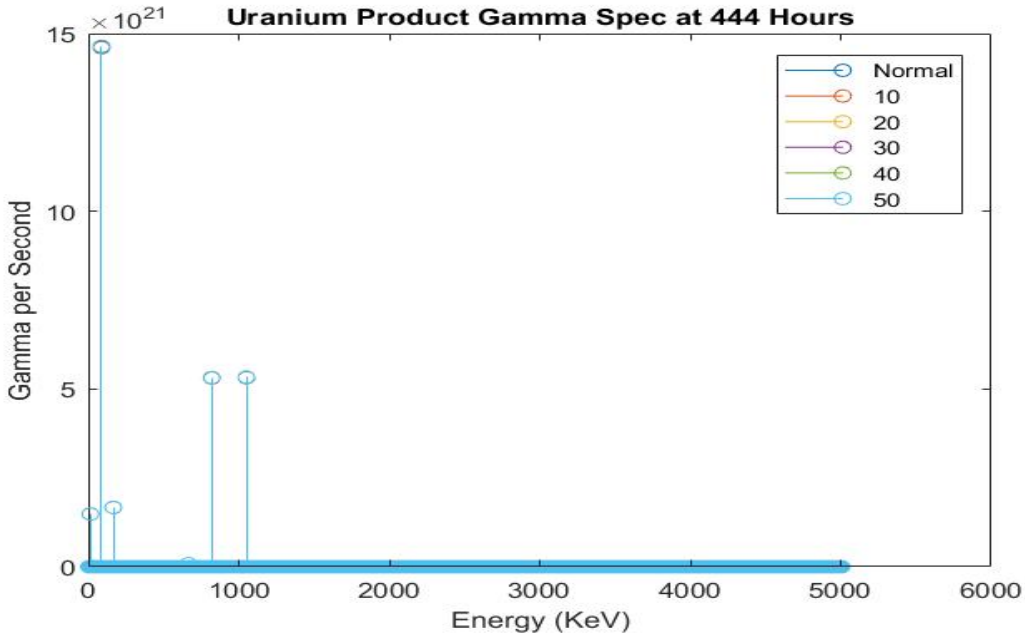

Figure 23: Gamma spectra at the U processing unit for different diversion scenarios.

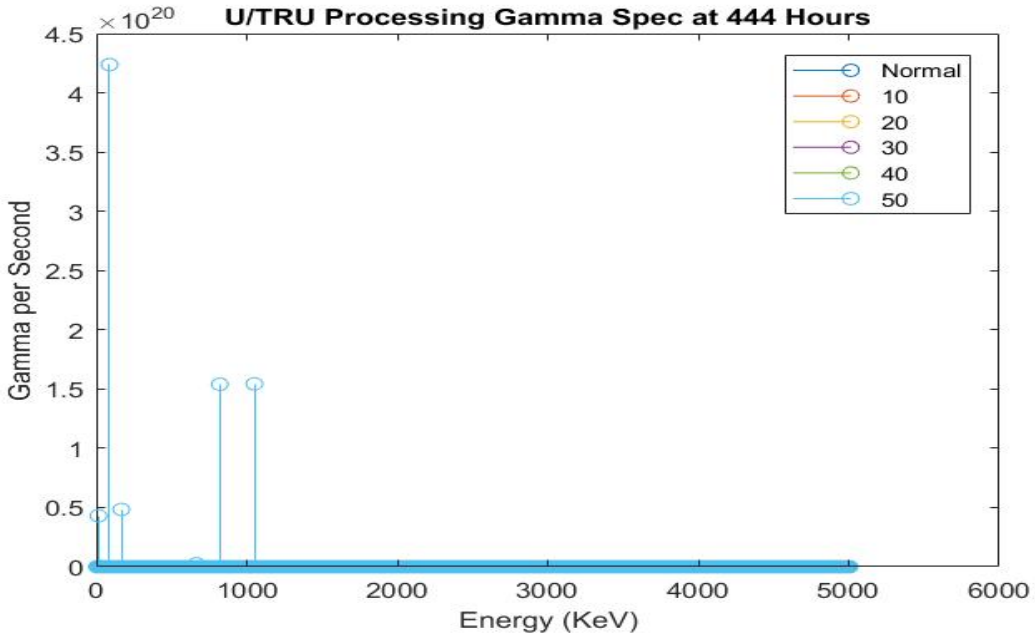

Figure 24: Gamma spectra at the UTRU processing unit for different diversion scenarios.

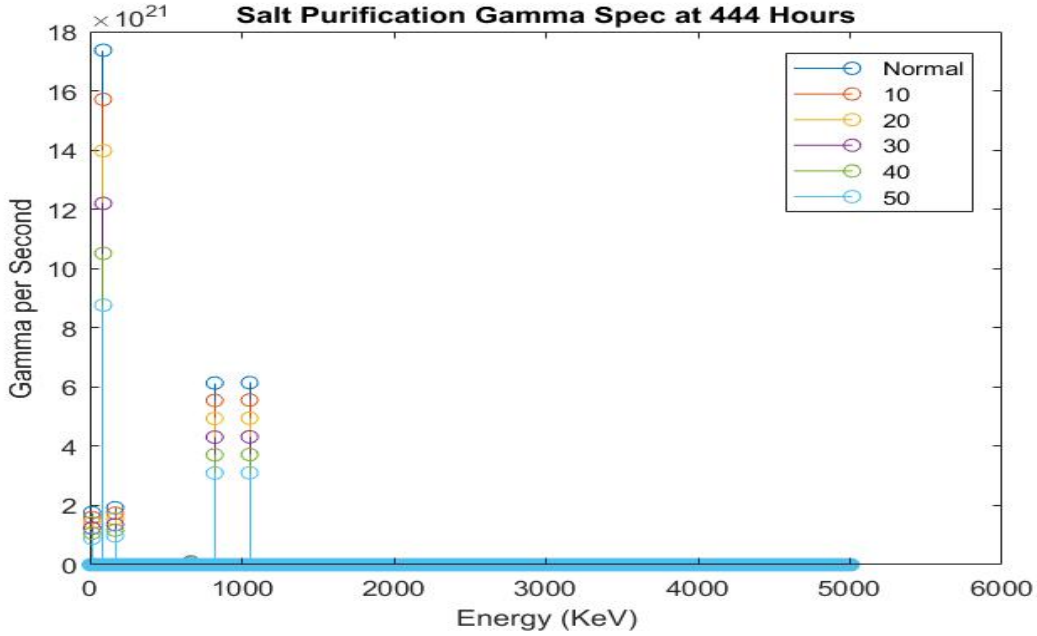

Figure 25: Gamma spectra for salt purification for different diversion scenarios.

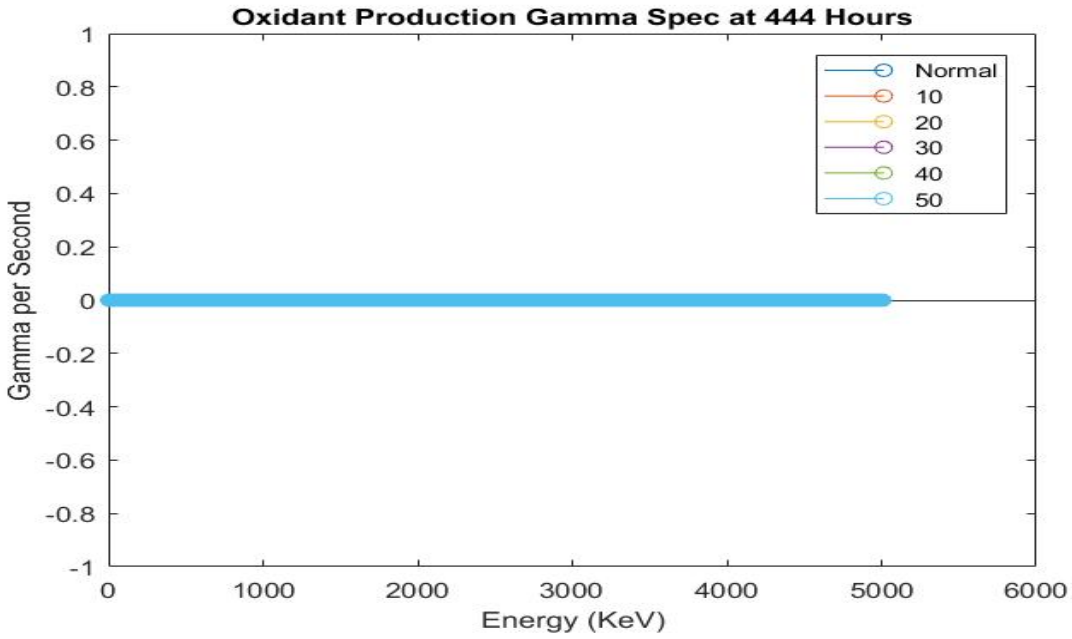

Figure 26: Gamma spectra for oxidant production for different diversion scenarios.

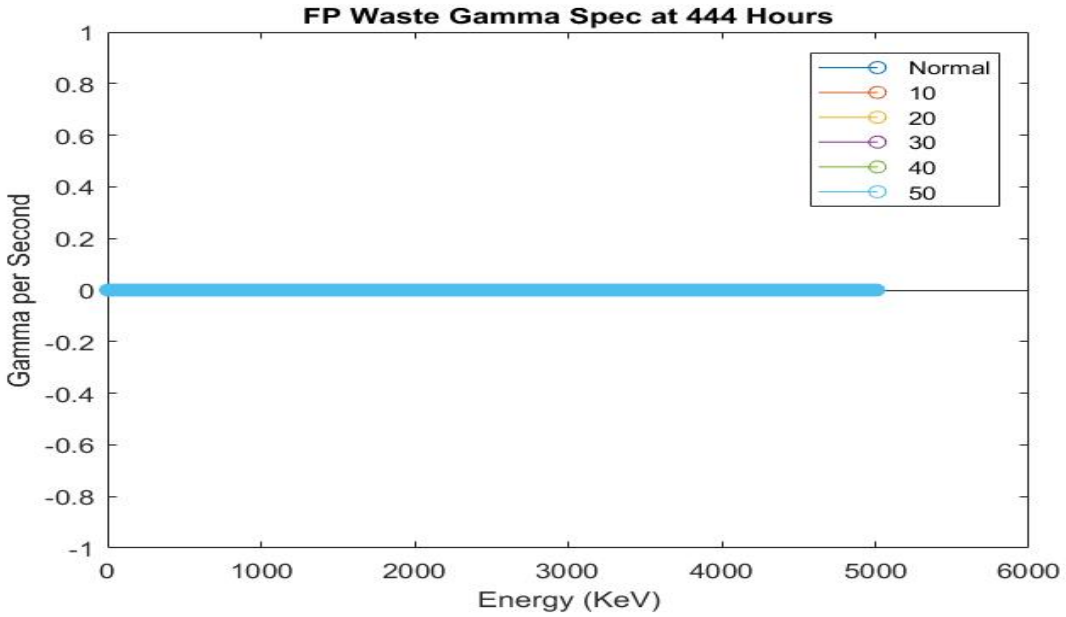

Figure 27: Gamma spectra at the fission product waste unit for different diversion scenarios.

Appendix B: Neutron Plots

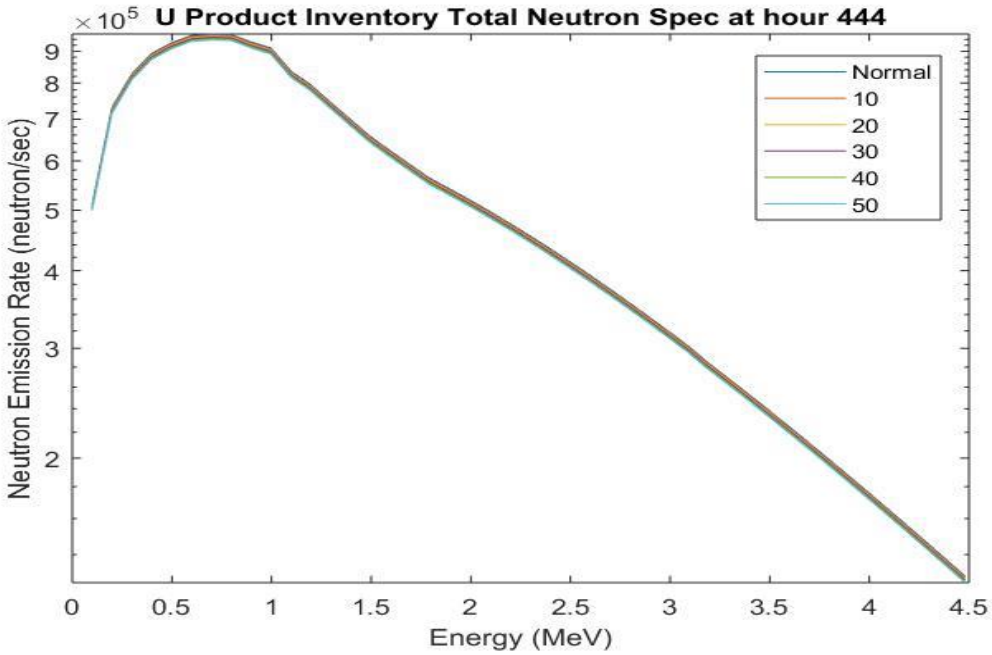

Figure 28: Total neutron spectra of the U processing unit for different diversion scenarios.

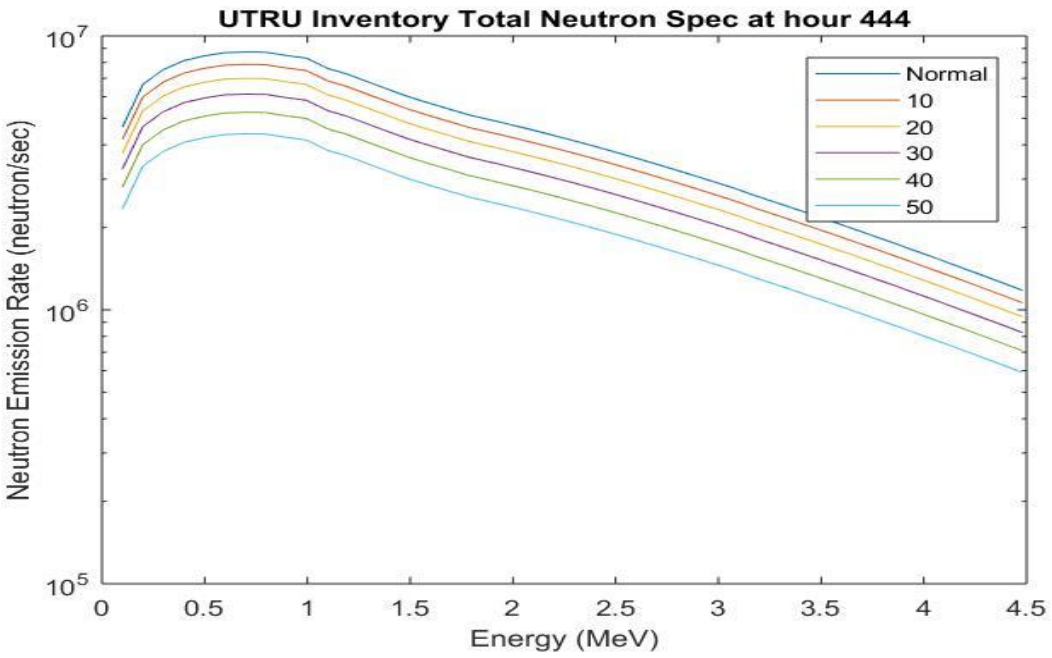

Figure 29: Total neutron spectra of the UTRU unit for different diversion scenarios.

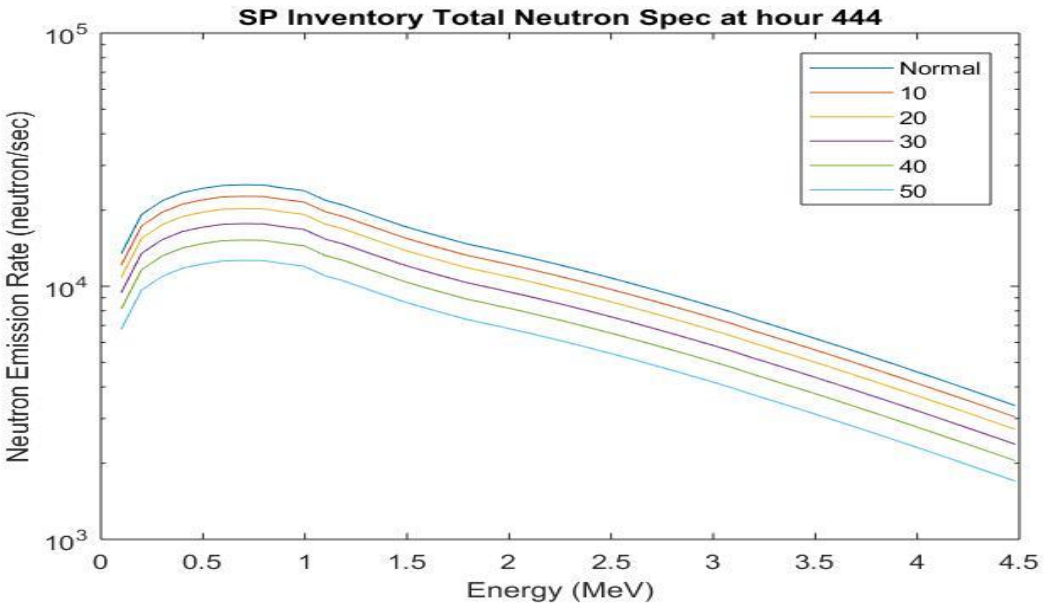

Figure 30: Total neutron spectra of the salt purification for different diversion scenarios.

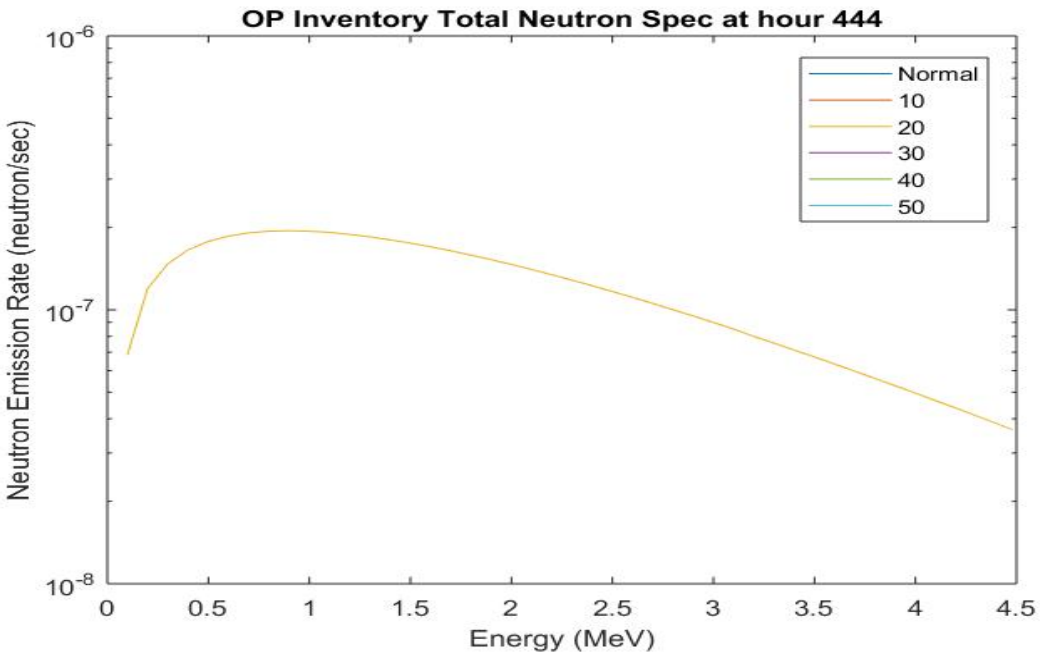

Figure 31: Total neutron spectra of the oxidant production for different diversion scenarios.

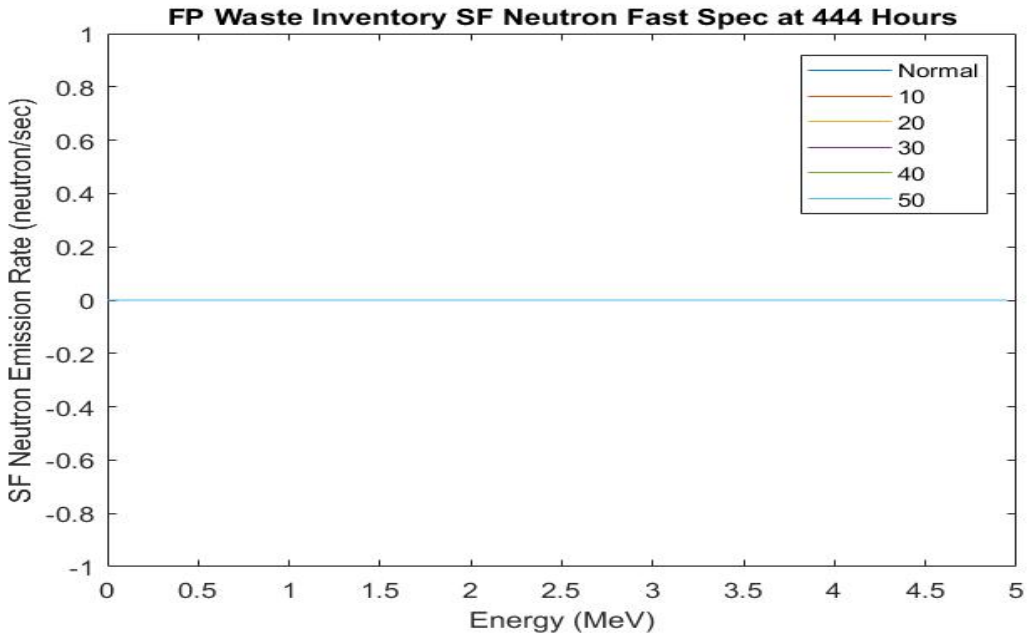

Figure 32: Total neutron spectra of the fission product waste for different diversion scenarios.

Appendix C: Diversion Ratios

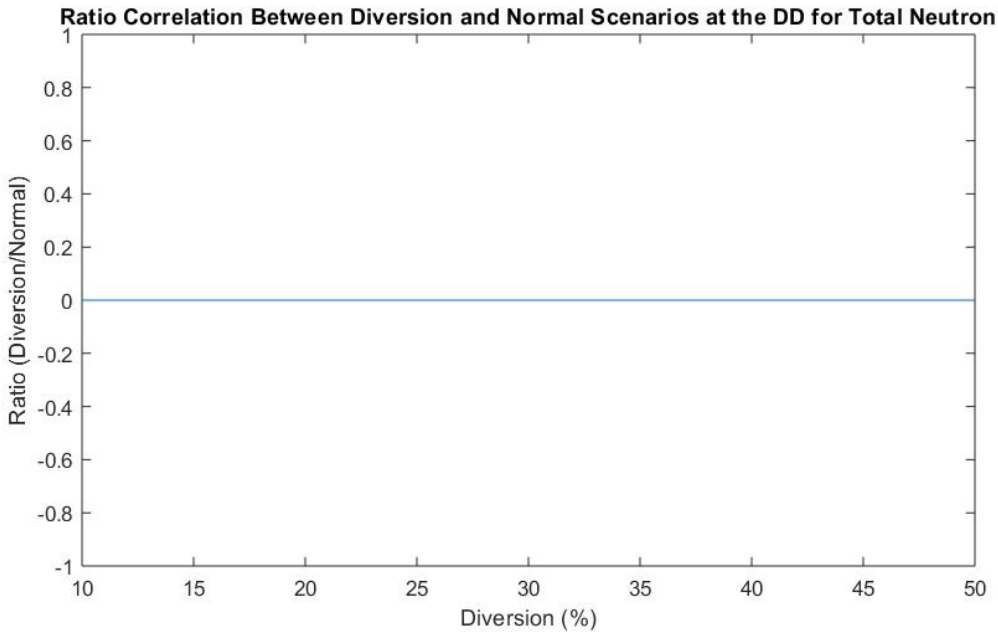

Figure 33: Ratio correlation between diversion scenarios at the drawdown unit for gamma emissions.

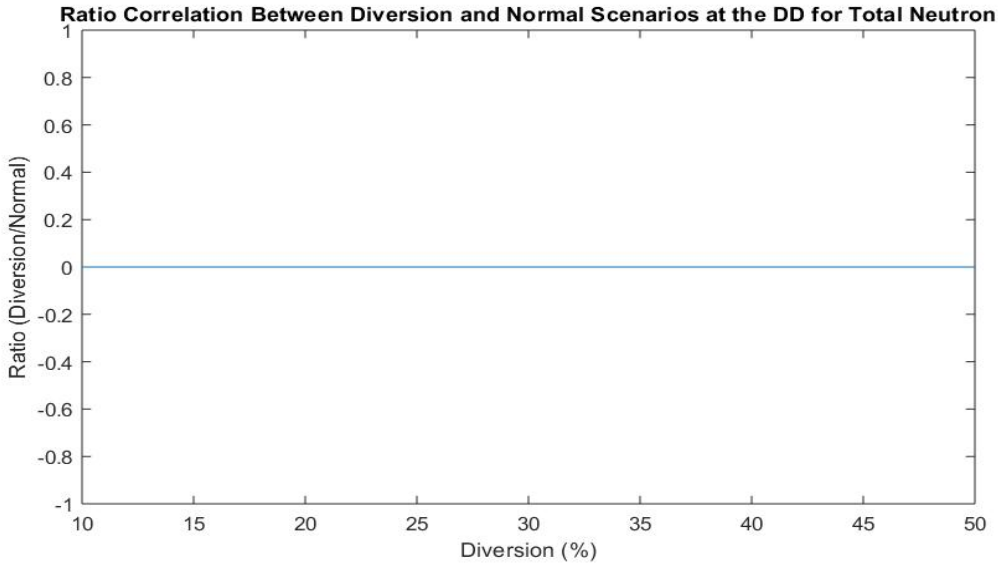

Figure 34: Ratio correlation between diversion scenarios at the drawdown unit for total neutron emissions.

VITA

Stephen N. Gilliam was born in Knoxville, TN to Steve and Kellie Gilliam. He is a triplet. He attended Central High School in Knoxville, TN. After graduation he spent four years at the University of Tennessee, finishing his undergraduate degree in Nuclear Engineering in May 2016. He accepted a graduate research assistantship at the University of Tennessee in the Nuclear Engineering program under his advisors Dr. Jamie Coble and Dr. Steve Skutnik. He graduates with his Master of Science degree in Nuclear Engineering in August 2018.